A Global Interactive Chemistry and Climate Model

Chien Wang, Ronald G. Prinn and Andrei P. Sokolov

Abstract

In order to elucidate interactions between climate change and biogeochemical processes and to provide a tool for comprehensive analysis of sensitivity, uncertainty, and proposed climate change mitigation policies, we have developed a zonally averaged two-dimensional model including coupled biogeochemical and climate sub-models, as a part of an Integrated Global System Model. When driven with calculated or estimated trace gas emissions from both anthropogenic and natural sources, it is designed to simulate centennial-scale evolution of many radiatively and chemically important tracers in the atmosphere. Predicted concentrations of chemical species in the chemistry sub-model are used interactively to calculate radiative forcing in the climate sub-model which in turn provides winds, temperatures, and other variables to the chemistry sub-model.

Model predictions of the surface trends of several key species are close to observations over the past 10-20 years. Predicted vertical distributions of climate-relevant species, as well as seasonal variations, are also in good agreement with observations. Runs of the model imply that, if the current increasing trends of anthropogenic emissions of climate-relevant gases are continued over the next century, the chemical composition of the atmosphere would be quite different in the year 2100 than that currently observed. The differences involve not only higher concentrations of major long-lived trace gases such as CO_2, N_2O, and CH_4, but also about 20% lower concentrations of the major tropospheric oxidizer (OH free radical), and almost double the current concentrations of the short-lived air pollutants CO and NO_x.

1. Introduction

Concerns about future climate change involve not only the impact of increases of long-lived trace gases in the atmosphere on the climate (*e.g.*, surface temperature, precipitation, and cloud coverage), but also the influence of climate change on atmospheric chemical processes and the possible effects of products of these processes, such as aerosols, on climate.

The lifetimes of chemical species in the atmosphere are affected by many processes, including atmospheric transport, chemical reactions, wet and dry deposition, exchange with the ocean or vegetation, and emissions from both human-related and natural processes. One needs to include treatment of each of these processes to address accurately the climatic effects of atmospheric chemical species and the influence of climate change on atmospheric chemistry. To address feedbacks between chemistry and climate it is clear that a coupled numerical model including explicit descriptions of both climate dynamics and atmospheric chemistry is needed.

In recent years, models addressing both climate and chemistry with various levels of coupling between these two components have been developed (*e.g.*, Hauglustaine, *et al.*, 1994; Taylor and Penner, 1994; Roelofts and Lelieveld, 1995; Moxim, *et al.*, 1996; Levy II, *et al.*, 1997). However, to quantify the magnitude and uncertainty of the effects on climate of long-lived trace gases (and *vice-versa*), a large number of long ($\geq$ 100 years) transient integrations using fully coupled models with special attention to surface fluxes need to be carried out. A model would in particular have to be computationally efficient so that many runs can be made in order to understand the relative importance of various climate-chemistry feedbacks, to determine sensitivity of the results to the many critical assumptions in sub-models, and (through comparison with observations) to make improvements. Constructing such a coupled model is both a theoretical and computational challenge.

Toward the goal of obtaining a better quantification of climate-chemistry interactions and their uncertainty, we have developed a coupled global-scale modeling system including a global climate model and an atmospheric chemistry model. This system is designed to predict as functions of time, latitude and altitude, the zonally-averaged concentrations of the major chemically and radiatively important trace species in the atmosphere. The chemistry and climate sub-models in this system are fully interactive. Specifically, the transport of chemical species is driven by dynamical variables predicted by the climate model and the calculations of gaseous and aqueous phase reactions are based on the temperatures, radiative fluxes, and precipitation rates computed in the climate model. Predicted mixing ratios of trace species are then used in turn to calculate the radiative forcing in the climate model.

This paper describes the coupled model in detail, with a special focus on the chemistry component which has not yet been published. Results from a 124-year 'reference' run and tests of the model using observational data are then presented. The last section provides a critique of these results and some conclusions. Further analyses focusing on the dynamics of the interactions between atmospheric chemistry and climate change are discussed in another paper.

2. Model Description

The climate sub-model used in the coupled model is the MIT two-dimensional (2D) land-ocean-resolving (LO) statistical-dynamical model (Sokolov and Stone, 1995, 1997). It is a modified version of a model developed at the Goddard Institute for Space Studies (GISS) (Yao and Stone, 1987; Stone and Yao, 1987, 1990). The original version of the 2D model was developed from the 3D GISS General Circulation Model (GCM) of Hansen, *et al.* (1983). As a result, the model's numerics and parameterizations of physical processes, such as radiation and convection, closely parallel those of the GISS GCM. The 2D-LO model solves the primitive equations as an initial value problem. The grid used in the model consists of 24 divisions in latitude (corresponding to a resolution of 7.826 degrees) and nine divisions in the vertical (two in the planetary boundary layer, five in the troposphere, and two in the stratosphere). The important feature of the 2D-LO model, from the point of view of coupling chemistry and climate dynamics, is the inclusion in its radiation code of all significant greenhouse gases, such as H_2O, CO_2, CH_4, N_2O, $CFCl_3$, CF_2Cl_2, and ozone, along with 12 types of aerosols.

One special aspect of this model is that its statistical-dynamical module for predicting climate is 20 times faster than three-dimensional models with similar latitudinal and vertical resolution. While two dimensional, it resolves the ocean and land separately at each latitude and reproduces many characteristics of the current zonally-averaged observed climate. The responses of this model to varies climate forcings are similar to those of three-dimensional GCMs. The 2D-LO model is already fully described in Sokolov and Stone (1995, 1997). The focus of this paper is primarily on the chemistry sub-model and on the coupling of these two sub-models.

Our chemistry sub-model is designed to use the same coordinate system as the climate sub-model. It has 25 chemical species including CO_2, CH_4, N_2O, O_3, CO, H_2O, NO_x, HO_x, SO_2, sulfate aerosol, and chlorofluorocarbons. Denoting zonally-averaged variables with over-bars and deviations from zonally-averaged variables with primes, the zonally-averaged mole fraction of any chemical species $\overline{C}$, is predicted by solving the following mass conserving equation:

$$\frac{\partial}{\partial t}\left(\frac{\overline{\Psi}}{mn}\right) = \overline{S}_{Advection} + \overline{S}_{Eddy} + \overline{S}_{Convection} + \overline{S}_{Emission} + \overline{S}_{Re\,action} + \overline{S}_{Deposition} \qquad [1]$$

where

$$\overline{\Psi} = \overline{\pi}\overline{C} \tag{2}$$

$$\overline{\pi} = \overline{P}_S - \overline{P}_T \tag{3}$$

$$\overline{S}_{Advection} = -\frac{\partial}{\partial \eta}\left(\frac{\overline{v}\overline{\Psi}}{m}\right) - \frac{\partial}{\partial \sigma}\left(\frac{\overline{\omega}\overline{\Psi}}{mn}\right) \tag{4}$$

$$m = (a\ COS\ \eta)^{-1} \tag{5}$$

$$n = a^{-1} \tag{6}$$

$$\sigma = \frac{\overline{P} - \overline{P}_T}{\overline{P}_S - \overline{P}_T} \tag{7}$$

$$\overline{\omega} = \frac{d\sigma}{dt} \tag{8}$$

Here, P_S, P, and P_T represent pressure at the surface, at an arbitrary grid point, and at the top of the atmosphere (fixed at 10 hPa), η is latitude, a is the Earth's radius, and v is the meridional wind speed. The right hand side of equation (Eq.) 1 includes all the major chemical source and sink terms, as well as the advective term as described by Eq. 4.

The continuity equations for $CFCl_3$, CF_2Cl_2, N_2O, O_3, CO, CO_2, NO, NO_2, N_2O_5, HNO_3, CH_4, CH_2O, SO_2, and H_2SO_4 include convergence due to transport (advection, eddy diffusion, and convection) whereas the remaining very reactive atoms, free radicals, or molecules are assumed to be unaffected by transport (photochemical steady-states) due to their very short lifetimes. Water vapor and air (N_2 plus O_2) densities are computed in the climate sub-model. The climate sub-model also provides the wind speeds, temperatures, solar radiative fluxes, and precipitation fluxes used in the chemical simulations.

2.1 Advection

The advection scheme is fourth-order and positive-definite (Wang and Chang, 1993; Wang and Crutzen, 1995), and based on a scheme suggested by Bott (1989a, b, 1993). It is used in a time-splitting procedure to calculate advection along each spatial dimension in order. Then a non-oscillating scheme is used to limit the numerical errors induced by possible overestimation of fluxes during the advective calculations (Smolarkiewicz and Grabowski, 1990). Finally, a mass adjustment for correcting the error induced by time-splitting and non-convergence-free wind fields is used (Kitada, 1987).

2.2 Eddy Diffusion and Convective Transport

The parameterization developed by Stone and Yao (1990) for meridional eddy diffusion of water vapor and temperature in zonally-averaged models has been used in this model for all transported chemical species.

From Stone and Yao (1990), the meridional component of the eddy flux ($\overline{v'\Psi'}$) is parameterized in terms of a horizontal diffusion coefficient K_{yy}, assuming that the motions related to baroclinic waves are quasi-horizontal:

$$\overline{v'\Psi'} \cong -K_{yy}\left(\frac{\partial \overline{\Psi}}{\partial y}\right) \tag{9}$$

The vertical component of the eddy flux is similarly obtained using the same formula and vertical eddy diffusion coefficient K_{zz} as proposed by Stone and Yao (1990) for water vapor.

To eliminate numerical noise and correct an apparent underestimate of the horizontal eddy fluxes in the tropical regions, we applied a second-order horizontal diffusion term in the model with a constant diffusion coefficient K_H of 8×10^5 m^2/s, which is significantly smaller than the typical eddy coefficients of 2 to 4×10^6 m^2/s in midlatitudes. Sensitivity runs have shown that, without this diffusion term, the model produces gradients of the passive tracer CFCl$_3$ defined by the differences between mole fractions in the midlatitudes of the Northern and Southern Hemispheres, which are to high compared to observations. Runs with this added weak diffusion as discussed later provide an excellent fit to this gradient and its evolution in time.

Vertical transport of chemical species by dry and moist convection is included, as well as vertical mixing by turbulence in the planetary boundary layer. These sub-grid scale processes are both treated using the same schemes used for water vapor in the climate model (Hansen, *et al.*, 1983).

2.3 Chemistry and Deposition

There are 41 gas-phase and 12 heterogeneous reactions in the model. The gas-phase chemistry has three major parts: tropospheric O$_3$-HO$_x$-NO$_x$-CO- CH$_4$ reactions (following Crutzen and Zimmermann, 1991), tropospheric SO$_2$-sulfate reactions, and stratospheric chlorofluorocarbon and N$_2$O removal reactions (Table 1). In its present form, the chemistry model uses specified stratospheric photochemical destruction rates computed off-line in recent runs of a global three-dimensional stratospheric model (Golombek and Prinn, 1986, 1993). The latter destruction rates yield global atmospheric life times of 46 years for CFCl$_3$, 120 years for CF$_2$Cl$_2$, and 150 years for N$_2$O.

We use the Livermore Solver for Ordinary Differential Equations, or LSODE (Hindmarsh, 1983), with certain modifications, to solve the characteristically stiff ordinary differential equations involved in modeling the tropospheric chemistry. To reduce the size of the matrix to be inverted in LSODE, we assume a quasi-steady state for the atoms and free radicals with very short lifetimes (*e.g.*, O(^{3}P), O(^{1}D), H, NO$_3$, CH$_3$, CHO, CH$_3$O, CH$_3$O$_2$, HOSO$_2$, and SO$_3$). Tests of the quasi-steady state assumption have been carried out using both a zero-dimensional "box" gas-phase chemistry model and our fully coupled climate and chemistry model. These tests show that the simplified version with quasi-steady states provides results very similar to a more comprehensive version without these approximations, and, greatly reduces the computational time.

Dissolution of soluble gases in precipitating water is included in the wet deposition term in the model (Table 2) and the precipitating water is removed at each time step assuming no further aqueous reactions. The impact of these heterogeneous reactions, therefore, is primarily on the gaseous phase component of chemical species. For a chemical species, the ratio of its gaseous phase to its aqueous phase component is (Seinfeld, 1986):

$$r = \frac{M(aq)}{M(g)} = \frac{HpL}{p/RT} = HRTL \qquad [10]$$

where $M(aq)$ is the aqueous phase concentration and $M(g)$ is the gaseous phase concentration, both in moles per liter of atmospheric air; p and H are the partial pressure (atm) and the effective Henry's Law coefficient (mole l^{-1} atm^{-1}) respectively of the species; R is the gas constant (0.082 atm mole l^{-1} K^{-1}); T is temperature in degrees K; and L is the volume of condensed water per unit volume of air, which is $\cong 10^{-3}$ times the molar mixing ratio of condensed water. If $M^0(g)$ represents the concentration of the species in the gas phase before the calculation of wet scavenging, the post-

scavenging gas phase concentration $M(g)$ can be derived from Eq. 10 combined with the requirement for conservation that $M(g) = M^0(g) - M(aq) = M^0(g) - r\,M(g)$ to yield

$$M(g) = \frac{M^0(g)}{1+r}$$ [11]

Dry deposition of some of the chemical species (NO, NO_2, HNO_3, N_2O_5, O_3, H_2O_2, and CH_3O_2H) has been formulated in this model based on previous work (Hough, 1991; Kanakidou, *et al.*, 1991; Hauglustaine, *et al.*, 1994).

2.4 Carbon Sinks

We have included two major net sinks of CO_2 in our model: land biospheric uptake (primarily by vegetation in the Northern Hemisphere) and oceanic uptake. A fixed value of 1.9 PgC per year is assumed for the current land biospheric uptake of CO_2 consistent with IPCC (1994) estimates. Runs of a terrestrial ecosystem model (Xiao, *et al.*, 1997) driven by rising CO_2 and changing climate have indicated that land uptake may vary with time (Prinn, *et al.*, 1997). This possibility will be addressed in later versions of the chemistry/climate model run interactively with the terrestrial ecosystem model. The oceanic uptake of CO_2 is calculated using an ocean carbon model (Prinn, *et al.*, 1997), which includes inorganic chemistry in the ocean surface water and transport of dissolved inorganic carbon to the deep ocean using the same scheme as used for heat in the 2D-LO climate sub-model.

The oceanic uptake of CO_2 at 22 latitudinal grid points (from 90 ˚N to 74 ˚S) are calculated each day by the ocean carbon sub-model based on the predicted surface winds, atmospheric concentrations of CO_2, and oceanic distributions of temperature and dissolved inorganic carbons. Predicted rates of this oceanic uptake are about 2.0 PgC/yr for the 1980s and increase thereafter to 8.4 PgC/yr in 2100. In the present version of our model, the land biospheric uptake (1.9 PgC/yr) is treated by removing appropriate amounts of CO_2 hourly at each grid point of the model with no attempt to simulate the substantial seasonal cycle in this uptake.

2.5 Emissions

Emissions of CO_2, CH_4, N_2O, $CFCl_3$, CF_2Cl_2, CO, NO, and SO_2 are considered. Except for the two chlorofluorocarbons, all emissions are divided into natural and anthropogenic emissions. Both are functions of latitude and include many sub-categories. Values for, and distributions of these emissions are based on previous research: Prinn, *et al.* (1990) for N_2O before 1990s; Hartley and Prinn (1993) for $CFCl_3$ and CF_2Cl_2 up to 1992; AFEAS (1993) and Fisher, *et al.* (1994) for $CFCl_3$ and CF_2Cl_2 after 1992; IPCC (1994) for CO_2; Fung, *et al.* (1991) for CH_4; Spiro, *et al.* (1992) for SO_2; Hough (1991), Law and Pyle (1993), and Crutzen and Zimmermann (1991) for CO and NO_X; and the GEIA data set (Graedel, 1994) for SO_2. Figure 1 shows the latitudinal distributions of emissions used in our simulations up to the year 1985. After 1985, latitudinal distributions of CO, NO, and SO_2 are predicted and change with time.

In the present simulations, the total annual natural emissions of CH_4, N_2O, CO, NO, and SO_2 are treated as constants with time. Specifically, the assumed natural emissions of CH_4, N_2O, CO, NO (exclusive of lightning), and sulfur are 130 Tg/yr, 9.1 Tg(N)/yr, 158.6 Tg(C)/yr, 10 Tg(N)/yr, and 12.8 Tg(S)/yr respectively. Production of NO by lightning is assumed to be 5 Tg(N)/yr in all years but distributed as a function of both latitude and season in each year (Kumar, *et al.*, 1995). Runs of a natural emissions model driven by changing climate and land ecosystems indicate significant changes in natural N_2O and CH_4 emissions are possible (Liu, 1996; Prinn, *et al.*, 1997). This will be studied in later versions of the chemistry/climate model.

The treatment of anthropogenic emissions other than chlorofluorocarbons consists of two parts: (1) from 1977 to 1985, and (2) after 1986. In the first period, the estimates are based on previous research results as listed above. For the second period the time-varying annual amounts of anthropogenic emissions predicted by the MIT Emissions Prediction and Policy Analysis (EPPA) Model in 12 economic regions (Yang, *et al.*, 1996) are mapped into emissions for each latitudinal grid point. For the emissions of chlorofluorocarbons before 1994, values from Hartley and Prinn (1993), AFEAS (1993), and Fisher, *et al.* (1994) are assumed. After 1994 emissions decrease linearly to zero values after the year 2000. To achieve reasonable mixing efficiency and numerical stability, all the emissions except for those of NO from lightning are added uniformly each day into the lowest two layers of the model.

2.6 Coupling of Sub-Models

The coupling of the chemistry and climate sub-models in the system is two-way (*i.e.*, fully interactive or on-line). The advection of chemical species is driven by the predicted winds provided by the climate sub-model every 20 minutes. The other transport processes (convection and eddy diffusion) and the wet and dry deposition rates are calculated every hour (*i.e.*, three times the climate sub-model time step). The gas-phase chemistry is solved with three-hour time steps using solar radiation fluxes, temperatures, and water vapor mixing ratios calculated by the climate sub-model. Predicted mole fractions of radiatively active gases, specifically CO_2, N_2O, CH_4, $CFCl_3$, CF_2Cl_2, and optical depths of sulfate aerosol, are used in turn every five hours by the climate sub-model to derive their contributions to radiative forcing. In the current version of the chemistry sub-model, the radiative forcing due to the predicted sulfate derived from anthropogenic SO_2 is applied as an additional forcing (both direct and indirect) to a constant background aerosol forcing in the climate sub-model. It is interpreted as the additional radiative forcing due to anthropogenic sulfur emissions and is applied only to the land fraction of the climate sub-model at each relevant latitude. The aerosol direct effect is computed from the predicted concentrations of sulfate aerosols. The highly uncertain indirect aerosol effect is parameterized by assuming radiative forcing by this effect is twice that computed for the direct effect, consistent with the recent IPCC (1996) assessment.

3. Reference Run

In order to test the model, we carried out a transient simulation of "present-day" conditions and a series of sensitivity tests using specified surface emissions of the relevant chemicals. The "present-day" simulation period begins in 1977, enabling use of observations (*e.g.*, Cunnold, *et al.*, 1994; Novelli, *et al.*, 1992) to compare with model results. Total integration times of these runs are 124 years (from 1977 to 2100).

Specified emissions for all the relevant species, including both natural and anthropogenic sources, used in these runs as functions of time are summarized in Fig. 2. Except for those of chlorofluorocarbons, which are assumed to decline linearly after 1994, all emissions increase with time (*e.g.*, N_2O from 12 TgN/yr in 1977 to 19 TgN/yr in 2100, CO_2 from 5.4 PgC/yr in 1977 to 21 PgC/yr in 2100, CH_4 from 540 Tg/yr in 1977 to 1.1 Pg/yr in 2100).

3.1 Temporal Trends

As a result of the assumed increasing emissions of long-lived gases, global average mole fractions of CO_2, N_2O, and CH_4 rise to 745 ppm, 410 ppb, and 4.4 ppm respectively by the year 2100. The model also predicts that if the actual reduction of $CFCl_3$ and CF_2Cl_2 emissions is the same as we assume in the model, the global average $CFCl_3$ and CF_2Cl_2 mole fractions will

decrease to their 1977 levels around 2030 and after 2090 respectively (the difference between the two being due to the much longer lifetime of CF_2Cl_2).

Climate sub-model results (Fig. 3) show that the global average surface temperature increases by about 2.5 °C between 1990 and 2100. This increase is due to the increased radiative forcing of the trace gases and subsequent climate-model feedbacks, and occurs despite the slightly enhanced cooling effect of increasing sulfate aerosols over this time. Global-annual-mean cloud coverage is predicted to drop by about 0.5% by the end of next century, while the global-mean annual precipitation increases from 2.92 mm/day in 1990 to 3.10 mm/day in 2100. Details of other aspects of climate-change patterns and impacts predicted by the 2D-LO model can be found in a separate article (Prinn, *et al.*, 1997).

Similar increases to the ones for the long-lived species are found for several short-lived species including CO, NO_x, SO_2, and sulfate, again driven primarily by their increased emissions. For example, the tropospheric average mole fraction of CO is predicted to be 180 ppb in 2100, which is about double the current value. For NO_x, in the lower atmosphere, wintertime surface mole fractions in midlatitudes of the Northern Hemisphere rise from 420 ppt in 1996 to 885 ppt in 2100. Increased emissions of SO_2 (57% according to Fig. 2) are offset somewhat by increased wet deposition associated with predicted rainfall increases. The maximum monthly mean value of the SO_2 surface mole fraction as seen in the midlatitudes of the Northern Hemisphere increased by about 18% from 1996 to 2100, while the same parameter for sulfate increased by about 42% during the winter and almost doubled in the summertime. Opposite to the trends of most short-lived species, the concentration of tropospheric OH, the most important oxidizing species in the lower atmosphere, is predicted to decrease by about 20% between 1990 and 2100 (Fig. 4). The decrease is due to the predicted increases of CH_4 and CO emissions (Fig. 2) and hence concentrations (Fig. 4), offset by increased NO_x emissions and modulated by changes in temperature and humidity.

3.2 Spatial Distributions

As expected, many short-lived species are predicted to have very strong spatial and seasonal variability. Predicted present-day CO concentrations for the Northern Hemisphere are much higher during the wintertime than the summertime (Fig. 5). Specifically, the peak value of the CO mole fraction in the middle and upper troposphere in the Northern Hemisphere is about 40 ppb lower in the summer than the winter. This seasonal difference, caused by more rapid summertime removal of CO, also affects the tropical region. Specifically, tropical and northern subtropical CO concentrations are much higher in northern hemisphere winter than summer at all tropospheric levels. Note also that, due to the high predicted concentrations of OH in the tropics, CO concentrations in the tropical region are lower than those even in the free troposphere over the Northern Hemisphere despite significant tropical CO emissions (Fig. 1).

The modeled NO_x ($NO + NO_2$) pattern has a similar seasonal variability to CO in the lower atmosphere in the Northern Hemisphere (Fig. 6). In addition, a very interesting feature of the predicted NO_x distribution is the appearance of a band of relatively high NO_x around the tropopause at low latitudes which changes little between seasons. The source of this band is both transport of NO_x from the lower atmosphere and local production by lightning (Fig. 7). Lacking observational data for tropical upper tropospheric NO_x, we can not confirm the reality of this prediction at this moment, although it turns out to be consistent with recent three-dimensional model results (Levy II, *et al.*, 1997). Note that the model does not include stratospheric downward transport of either NO_x or NO_y.

Regions with predicted high mole fractions of OH switch from the Northern Hemisphere summer to the Southern Hemisphere summer, following the movement of the tropical convective zone (Fig. 8). The high OH in the tropical upper troposphere results from the enhanced NO_x levels and ultraviolet fluxes as well as ample H_2O and O_3 levels. Note that the concentrations predicted for OH in the upper troposphere are somewhat lower than those estimated by Prinn, *et al.* (1995), which are based on CH_3CCl_3 observations.

From Fig. 9 we see that the seasonal variations of the SO_2 distribution are not as dramatic as those for CO and NO_x, particularly in lower troposphere (below 634 hPa). Because the major sinks of SO_2 in this model are the conversion to sulfate and wet deposition, we can therefore draw the conclusion that the combination of these two processes approximately balance both regionally and seasonally the emissions of SO_2 (see Fig. 1). In contrast to this pattern, the sulfate distribution is quite different in different seasons (Fig. 10). The primary reason is the seasonal variation in its production by the OH, SO_2 reaction and its very high solubility. Strong wet scavenging of sulfate gives it a short life time in the atmosphere and the long-range transport of sulfate is therefore negligible.

4. Comparison with Observations

4.1 Long-lived Species

Long-lived species, such as $CFCl_3$, CF_2Cl_2, N_2O, and CO_2, are predicted and observed to be generally well-mixed vertically in the free troposphere. Latitudinal gradients of their concentrations exist however because of the latitudinal distributions of their sources with the magnitude of the gradient dependent upon the rate of north-south transport. Therefore, comparisons of their observed and predicted surface mixing ratios as functions of latitude and time are a very good measure of the accuracy of horizontal transport rates in the model provided the latitudinal distributions of emissions are known. For this purpose, we have used the emissions discussed earlier in Section 2.5 together with monthly-mean measurements from the surface networks of ALE/GAGE/AGAGE (for $CFCl_3$, CF_2Cl_2, and N_2O) and NOAA/CMDL (for CO_2) to compare with the outputs of our model at the same latitudes and times.

We found that simulated temporal trends and latitudinal gradients in $CFCl_3$ and CF_2Cl_2 surface mole fractions agree very well with observations at the five ALE/GAGE/AGAGE stations (Figs. 11 and 12). Because the sources of these two chlorofluorocarbons are predominately in the Northern Hemisphere, this agreement demonstrates that the simulation of inter-hemispheric transport in the model is quite reasonable. The variations in time of the predicted and measured latitudinal gradients of these species (as measured by the difference between the Ireland and Tasmania stations) also agree very well; for $CFCl_3$ this difference has decreased both in the model and in observations from 15 to 20 pptv before 1990 to 5 pptv in 1995 consistent with the rapid reduction in Northern Hemisphere emissions of this compound. The good agreement between predicted and observed global average concentrations indicates that the model parameterization for stratospheric losses of these species is also reasonable.

The vertical distributions of long-lived species predicted in the model have been compared with three balloon observations at 44 °N (June 20, 1989; November 5 and 10, 1990) by Ulrich Schmidt and co-workers as reported in Fraser, *et al.* (1994). The model data were averaged values from June 1989 to November 1990. For the comparison, both observational and modeled mole fractions were expressed relative to the maximum values in each profile (Fig. 13). The observed and modeled $CFCl_3$ profiles so normalized are quite close in shape, although differences as high as 10% can be found at some levels.

Our model also predicts trends of the surface mole fractions of N_2O which are close to the ALE/GAGE/AGAGE observations, especially in the Southern Hemisphere and the Tropics (Fig. 14). In the Northern Hemisphere midlatitudes, the simulated N_2O mixing ratios are generally lower than the observed ones although the predicted trends are still similar to observations. A probable reason for this result is underestimation of the N_2O emissions in the Northern Hemisphere midlatitudes.

The model predicts oceanic uptake of carbon dioxide (~2.0 PgC/yr for the 1980s) close to the values predicted in the more detailed models (*e.g.*, 1.81 PgC/yr in Sarmiento*, et al.*, 1992; 2.1 PgC/yr in Orr, 1993; both are for the 1980s), and together with the assumed terrestrial CO_2 uptake, this leads to predicted trends for the surface mole fractions of CO_2 close to those observed at five globally distributed NOAA/CMDL stations (Fig. 15). Note that the seasonal cycles in predicted concentrations are due to transport and oceanic uptake only. The seasonal cycle in the net terrestrial biospheric flux (positive in fall and winter and negative in spring and summer in the Northern Hemisphere) is not included as noted earlier. Fully interactive coupling of the ecosystem model with the current chemistry/climate model is underway and hopefully will provide a realistic representation of this missing cyclical process.

4.2 CH$_4$ and CO

When compared to the ALE/GAGE/AGAGE network measurements, the surface mole fractions of CH_4 predicted in our model are generally quite close to the observations but are somewhat higher (by up to 0.1 ppm) than measured results at Samoa, Barbados, Oregon, and Ireland (Fig. 16). Over-prediction of CH_4 could be related to over-prediction of annual-average emissions or under-prediction of annual-average OH levels in the Northern Hemisphere. Predicted seasonal cycles at all five stations agree fairly well with observations indicating that the predicted seasonal cycles in transport and OH concentrations at the latitudes of these stations are quite realistic.

The major sink for atmospheric carbon monoxide is also reaction with OH and its lifetime is much shorter (months) relative to methane (8.3 years, Prinn, *et al.*, 1995). Therefore, zonal variations (not of course included in our model) are much larger for CO than for the long-lived species. The most we can expect from our zonal-mean model is an adequate simulation of latitudinal gradients and seasonal cycles in CO. Hence, model predictions and observations for CO at stations at specific longitudes are not expected to agree closely. We find in fact that the predicted annual-average mole fractions and seasonal variations of CO are more reasonable in the Northern Hemisphere than the Southern Hemisphere (Fig. 17, observational data are from the NOAA/CMDL network, see Novelli*, et al.*, 1992). Specifically, the model simulates the phase of the seasonal cycles at Alaska, Colorado, Mauna Loa, and Tasmania but under-predicts the amplitude of these cycles at Mauna Loa. Over-prediction of annual average concentrations particularly in the Tropics and Southern Hemisphere could be due to under-prediction of OH or to the assumed CO sources in these regions in the model being too large. It is interesting to note that a similar overestimation in simulating short-lived species is also found in other zonally-averaged models (*e.g.*, Derwent, 1996).

4.3 Tropospheric Ozone and OH

Ozone is one of the key species in tropospheric chemistry. However, due to its sometimes rapid *in situ* production and short life time in the troposphere, an adequate measurement network for tropospheric ozone requires fairly high spatial and temporal resolution and a carefully designed

distribution of stations (Prinn, 1988). Currently, such a network does not exist globally, but there are some observations available that are useful for partial model testing.

We specifically use the ozone sounding data archived in the World Ozone Data Center for 22 selected stations, which were operated after the late 1970s and covered a wide range of latitudes to compare with our model. Since the launching times and data retrieval levels are not standardized in the data set, we choose the surface and the 500 hPa levels for comparisons because both appeared in most launch records. We then derive the monthly means of these observations in order to compare with our modeling results at the same time and location (both latitudinally and vertically).

Figure 18 shows the correlation between model and observations. In the surface layer, data are generally symmetrically distributed about the linear relation line, but less so for data from midlatitude Northern Hemisphere stations (marked by blue "+" label) than for other stations (marked by red "O" label). It indicates that although the model not surprisingly overestimates or underestimates ozone concentrations at some specific stations and times, it does reproduce the general climatology of the latitudinal distribution of ozone outside of polluted regions. At the 500 hPa level, the model clearly underestimates O_3 mole fractions in the Northern Hemisphere midlatitudes but is again closer to observations in other regions. One plausible reason for these results is the geographical location of the stations. Since most of these stations are located in urban areas or close to urban areas, they may be poor representations of the zonal averages predicted in our model at polluted latitudes.

As a chemical cleaner and reaction mediator, OH is arguably the most important free radical in atmospheric chemistry. The globally-averaged OH concentration in the troposphere in our model for the current time (1995) is 10.4×10^5 radical/cm^3, which is quite close to the most recent estimate of $(9.7 \pm 0.6) \times 10^5$ radicals/cm^3 based on measurements of CH_3CCl_3 (Prinn, *et al.*, 1995). More detailed analysis indicates that the model slightly overestimates OH concentrations in the lower troposphere but underestimates them in the upper troposphere compared with the concentrations deduced in the eight tropospheric boxes in the Prinn, *et al.* (1995) analysis. Overall, the OH distributions predicted by this model provide reasonable simulations of OH-sensitive species as shown for CH_4 and CO in the earlier section, and also in an independent study using our model for CH_3CCl_3 (J. Huang, personal communication).

5. Conclusions

In order to investigate interactions between long-term changes in anthropogenic emissions and climate and biogeochemical processes, we have developed a zonally averaged two-dimensional model including coupled biogeochemical and climate sub-models. This model is itself a part of the MIT Integrated Global System Model (IGSM, Prinn, *et al.*, 1997). This model takes emissions of multiple gases from both anthropogenic and natural sources as inputs, and predicts transport, photochemical rates, and deposition fluxes, in order to simulate evolution of many radiatively and chemically important species in the atmosphere. Predicted concentrations of chemical species are used in a fully interactive procedure to calculate radiative forcing in the climate sub-model. In the study of the centennial-scale climate change problem, the model has been shown to be a numerically efficient tool while retaining most of the important processes in a self-consistent and comprehensive way.

As shown from the results of a 'reference' run designed to be comparable to the IPCC IS92a scenario for CO_2 emissions, significant changes in concentrations of climate-relevant gases and hence in climate variables are predicted. The modeled current-day multi-year surface trends of several key long-lived species are generally close to observational data. Simulated vertical

distributions of long-lived species are also in reasonable agreement with observations. For shorter-lived species, a direct comparison between modeled results and individual station measurements show differences that we believe can be attributed in part to the zonal-averaging in the model and in part to emission uncertainties. At the same time, this model provides reasonable simulations of seasonal variability and good agreement with observations in high northern latitudes. The agreements where they exist, do not of course guarantee that the model will exactly represent the future evolution of the atmosphere. It does however provide some confidence in the transport and chemistry along with other features in the model, and in provides a platform for analyzing sensitivities and uncertainties. In addition, this model should be a useful tool for analyzing policies proposed to lower emissions.

Modeled results indicate that if the current increasing trends of anthropogenic emissions of climate-relevant gases are continued into the next century, the chemical structure of the atmosphere at the end of the next century would be quite different from the one we have now. The differences include significantly higher concentrations in 2100 of major trace gases such as CO_2 (745 ppmv), N_2O (410 ppbv), and CH_4 (4.4 ppmv), lowered concentrations of tropospheric OH radicals (20% decrease from the current level), and almost doubled concentrations from the current levels for the shorter-lived species CO and NO_x. As a result of this modified chemical composition, we predict a significantly warmer climate and increased precipitation, despite the cooling effect of aerosols included in the model.

Among the more interesting results from this model is the quantification of the two-way feedback between climate dynamics and atmospheric chemistry. Changes in climate, specifically in H_2O, temperature, and rainfall, provide different photochemical production and loss rates for many chemical species, while modified chemical concentrations in the atmosphere also significantly impact the climate. These results will be discussed in more detail in another paper.

It is obvious that there are many uncertainties in a model of this type. These uncertainties include, to name a few, effects of zonal-averaging, oceanic dynamics and interaction with the atmosphere, the sulfate aerosol effect on the radiation, stratosphere-troposphere exchange (especially when related to ozone), and the effect of the neglected contributions of non-methane hydrocarbons (many of them relate to polluted regions) on tropospheric chemistry. To narrow these uncertainties, further work is needed.

Acknowledgments

References

AFEAS (Alternative Fluorocarbons Environmental Acceptability Study), Production, Sales and Atmospheric Release of Fluorocarbons Through 1994, AFEAS Administrative Organization, Washington, D.C., 1994.

Atkinson, P.S., D.L. Baulch, R.A. Cox, R.S. Hampson, Jr., J.A. Kerr and J. Troe, Evaluated kinetic and photochemical data for atmospheric chemistry, *J. Phys. Chem. Ref. Data*, 21(6), 1125-1444, 1992.

Bott, A., A positive definite advection scheme obtained by nonlinear renormalization of the advective fluxes, *Mon. Wea. Rev*., 117, 1006-1015, 1989a.

Bott, A., Reply to Smolarkiewicz's comment, *Mon. Wea. Rev.*, 117, 2633-2636, 1989b.

Bott, A., The monotone area-preserving flux-form advection algorithm: Reducing the time-splitting error in two-dimensional flow fields, *Mon. Wea. Rev*., 121, 2637-2641, 1993.

Crutzen, P.J., and P.H. Zimmermann, The changing photochemistry of the troposphere, *Tellus*, 43AB, 136-151, 1991.

Cunnold, D.M., P.J. Fraser, R.F. Weiss, R.G. Prinn, P.G. Simmonds, B.R. Miller, F.N. Alyea and A.J. Crawford, Global trends and annual releases of CCl_3F and CCl_2F_2 estimated from ALE/GAGE and other measurements from July 1978 to June 1991, *J. Geophys. Res*., 99, 1107-1126, 1994.

DeMore, W.B., S.P. Sander, D.M. Golden, R.F. Hampson, M.J. Kurylo, C.J. Howard, A.R. Ravishankara, C.E. Kolb and M.J. Molina, Chemical kinetics and photochemical data for use in stratospheric modeling. Evaluation Number 11, JPL Publication, Report No. 94-26, 1994.

Derwent, R. G., The influence of human activities on the distribution of hydroxyl radicals in the troposphere, *Phil. Trans. R. Soc. Lond.* A, 354, 501-531.

Fraser, P., M. Gunson, S. Penkett, F.S. Rowland, U. Schmidt and R. Weiss, Measurements. Report on Concentrations, Lifetimes, and Trends of CFCs, Halons, and Related Species, NASA Reference Publication 1339, 1994.

Fisher, D.A., T. Duafala, P.M. Midgley and C. Niemi, Production and Emission of CFCs, Halons, and Related Molecules. Report on Concentrations, Lifetimes, and Trends of CFCs, Halons, and Related Species, NASA Reference Publication 1339, 1994.

Fung, I., *et al.*, Three-dimensional model synthesis of the global methane cycle, *J. Geophys. Res*., 96, 13,033-13,065, 1991.

Graedel, T.E., Global emission inventories to aid atmospheric modelers, *EOS* (Trans. AGU), 75, 585, 1994.

Golombek, A., and R.G. Prinn, A global three-dimensional model of the circulation and chemistry of $CFCl_3$, CF_2Cl_2, CH_3CCl_3, CCl_4, and N_2O, *J. Geophys. Res*., 91(D3), 3985-4001, 1986.

Golombek, A., and R.G. Prinn, A global three-dimensional model of the stratospheric sulfuric acid layer, *J. Atmos. Chem.*, 16, 179-199, 1993.

Hansen, J., G. Russel, D. Rind, P.H. Stone, A. Lacis, S. Lebedeff, R. Ruedy and L. Travis, Efficient three-dimensional global models for climate studies: Model I and Model II, *Mon. Wea. Rev*., 111, 609-662, 1983.

Hartley, D., and R.G. Prinn, Feasibility of determining surface emissions of trace gases using an inverse method in a three-dimensional chemical transport model, *J. Geophys. Res*., 98, 5183-5198, 1993.

Hauglustaine, D.A., C. Granier, G.P. Brasseur and G. Megie, The importance of atmospheric chemistry in the calculation of radiative forcing on the climate system, *J. Geophys. Res*., 99, 1173-1186, 1994.

Hindmarsh, A.C., ODEPACK, A systematized collection of ODE solvers, *Scientific Computing*, 55-64, R.S. Stepleman, *et al.* (eds.), North-Holland, Amsterdam, 1983.

Hough, A.M., Development of a two-dimensional global tropospheric model: Model chemistry, *J. Geophys. Res.*, 96, 7325-7362, 1991.

IPCC, Climate Change 1994: Radiative Forcing of Climate Change and an Evaluation of the IPCC IS92 Emission Scenarios, Cambridge Univ. Press, Cambridge, UK, 339 p, 1994.

IPCC, Climate Change 1995: The Science of Global Change, Cambridge Univ. Press, Cambridge, UK, 572 p, 1996.

Kanakidou, M., H.B. Singh, K.M. Valentin and P.J. Crutzen, A two-dimensional study of ethane and propane oxidation in the troposphere, *J. Geophys. Res.*, 96(D8), 15,395-15,413, 1991.

Kitada, T., Effect of non-zero divergence wind fields on atmospheric transport calculations, *Atmos. Environ.*, 21, 785-788, 1987.

Kumar, P.P., G.K. Manohar and S.S. Kandalgaonkar, Global distribution of nitric oxide produced by lightning and its seasonal variation, *J. Geophys. Res.*, 100, 11,203-11,208, 1995.

Law, K.S., and J.A. Pyle, Modeling trace gas budgets in the troposphere. 1. Ozone and odd nitrogen, *J. Geophys. Res.*, 98, 18,377-18,400, 1993.

Levy II, H., W.J. Moxim and P.S. Kasibhatla, A global three-dimensional time-dependent lightning source of tropospheric NO_x, *J. Geophys. Res.*, in press, 1997.

Levy II, H., P.S. Kasibhatla, W.J. Moxim, A.A. Klonecki, A.I. Hirsch, S.J. Oltmans and W.L. Chameides, The human impact on global tropospheric ozone, submitted to *Geophys. Res. Lett.*, 1997.

Liu, Y., Modeling the emissions of nitrous oxide (N_2O) and methane (CH_4) from the terrestrial biosphere to the atmosphere, MIT Joint Program on the Science and Policy of Global Change, Report No. 10, 219 p, 1996.

Moxim, W.J., H. Levy II and P.S. Kasibhatla, Simulated global tropospheric PAN: Its transport and impact on NO_x, *J. Geophys. Res.*, 101(D7), 12,621-12,638, 1996.

Novelli, P.C., L.P. Steele and P.P. Tans, Mixing ratio of carbon monoxide in the troposphere, *J. Geophys. Res.*, 97(D18), 20,731-20,750, 1992.

Orr, J.C., Accord between ocean models predicting uptake for anthropogenic CO_2, *Water, Air, and Soil Pollution*, 70, 465-481, 1993.

Pandis, S.N., and J.H. Seinfeld, Sensitivity analysis of chemical mechanism for aqueous-phase atmospheric chemistry, *J. Geophys. Res.*, 94, 1105-1126, 1989.

Prinn, R.G., Toward an improved global network for determination of tropospheric ozone climatology and trends, *J. Atmos. Chem.*, 6, 281-298, 1988.

Prinn, R.G., D. Cunnold, R. Rasmussen, P. Simmonds, F. Alyea, A. Crawford, P. Fraser, and R. Rosen, Atmospheric emissions and trends of nitrous oxide deduced from 10 years of ALE-GAGE data, *J. Geophys. Res.*, 95, 18,369-18,385, 1990.

Prinn, R.G., R.F. Weiss, B.R. Miller, J. Huang, F.N. Alyea, D.M. Cunnold, P.J. Fraser, D.E. Hartley and P.G. Simmonds, Atmospheric trends and lifetime of CH_3CCl_3 and global OH concentrations, *Science*, 269, 187-192, 1995.

Prinn, R.G., H. Jacoby, A. Sokolov, C. Wang, X. Xiao, Z. Yang, R. Eckaus, P. Stone, D. Ellerman, J. Melillo, J. Fitzmaurice, D. Kicklighter, G. Holian and Y. Liu, Integrated global system model for climate policy assessment: Feedbacks and sensitivity studies, submitted to *Climatic Change*, 1997.

Roelofs, G.-J., and J. Lelieveld, Distribution and budget of O_3 in the troposphere calculated with a chemistry general circulation model, *J. Geophys. Res.*, 100, 20,983-20,998, 1995.

Sarmiento, J.L., J.C. Orr and U. Siegenthaler, A perturbation simulation of CO_2 uptake in an ocean general circulation model, *J. Geophys. Res.*, 97, 3621-3645, 1992.

Seinfeld, J.H., Atmospheric Chemistry and Physics of Air Pollution, John Wiley, New York, 1986.

Smolarkiewicz, P.K., and W.W. Grabowski, The multidimensional positive definite advection transport algorithm: Nonoscillatory option, *J. Comput. Phys.*, 86, 355-375, 1990.

Sokolov, A.P., and P.H. Stone, Description and validation of the MIT version of the GISS 2D Model, MIT Joint Program on the Science and Policy of Global Change, Report No. 2, 46 p, 1995.

Sokolov, A.P., and P.H. Stone, A flexible climate model for use in integrated assessments, MIT Joint Program on the Science and Policy of Global Change, Report No. 17, 16 p, 1997; submitted to *Climatic Change*.

Spiro, P.A., D.J. Jacob and J.A. Logan, Global inventory of sulfur emissions with $1° \times 1°$ resolution, *J. Geophys. Res.*, 97, 6023-6036, 1992.

Stockwell, W.R., On the $HO_2 + HO_2$ reaction: Its misapplication in atmospheric chemistry models, *J. Geophys. Res.*, 100, 11,695-11,698, 1995.

Stone, P.H., and M.S. Yao, Development of a two-dimensional zonally averaged statistical-dynamical model, Part II: The role of eddy momentum fluxes in the general circulation and their parameterization, *J. Atmos. Sci.*, 44, 3769-3786, 1987.

Stone, P.H., and M.S. Yao, Development of a two-dimensional zonally averaged statistical-dynamical model, Part III: The parameterization of the eddy fluxes of heat and moisture, *J. Climate*, 3, 726-740, 1990.

Taylor, K.E., and J.E. Penner, Response of the climate system to atmospheric aerosols and greenhouse gases, *Nature*, 369, 734-737, 1994.

Wang, C., and J.S. Chang, A three-dimensional numerical model of cloud dynamics, microphysics, and chemistry. 1. Concepts and formulation, *J. Geophys. Res.*, 98, 14,827-14,844, 1993.

Wang, C., and P.J. Crutzen, Impact of a simulated severe local storm on the redistribution of sulfur dioxide, *J. Geophys. Res.*, 100, 11,357-11,367, 1995.

Xiao, X., D.W. Kicklighter, J.M. Melillo, A.D. McGuire, P.H. Stone and A. Sokolov, Linking a global terrestrial biogeochemical model and a 2-dimensional climate model: Implications for the global carbon budget, *Tellus*, 49B, 18-27, 1997.

Yang, Z., R.S. Eckaus, A.D. Ellerman and H.D. Jacoby, The MIT Emissions Prediction and Policy Analysis (EPPA) Model, MIT Joint Program on the Science and Policy of Global Change, Report No. 6, 49 p, 1996.

Yao, M.S., and P.H. Stone, Development of a two-dimensional zonally averaged statistical-dynamical model, Part I: The parameterization of moist convection and its role in the general circulation, *J. Atmos. Sci.*, 44, 65-82, 1987.

Table 1. Gaseous Phase Chemical Reactions Included in the Model

No.	Reactions	References for Rate Constants
R1	$O_3 + h\nu \rightarrow O(^1D) + O_2$	DeMore, *et al.* (1994)
R2	$O(^1D) + H_2O \rightarrow 2OH$	DeMore, *et al.* (1994)
R3	$O(^1D) + N_2 \rightarrow O + N_2$	DeMore, *et al.* (1994)
R4	$O(^1D) + O_2 \rightarrow O + O_2$	DeMore, *et al.* (1994)
R5	$CO + OH \rightarrow H + CO_2$	Atkinson, *et al.* (1992)
R6	$H + O_2 + M \rightarrow HO_2 + M$	Atkinson, *et al.* (1992)
R7	$HO_2 + NO \rightarrow OH + NO_2$	DeMore, *et al.* (1994)
R8	$NO_2 + h\nu \rightarrow NO + O$	DeMore, *et al.* (1994)
R9	$O + O_2 + M \rightarrow O_3 + M$	Atkinson, *et al.* (1992)
R10	$HO_2 + O_3 \rightarrow OH + 2O_2$	Atkinson, *et al.* (1992)
R11	$OH + O_3 \rightarrow HO_2 + O_2$	Atkinson, *et al.* (1992)
R12	$NO + O_3 \rightarrow NO_2 + O_2$	Atkinson, *et al.* (1992)
R13	$NO_2 + OH + M \rightarrow HNO_3 + M$	Atkinson, *et al.* (1992)
R14	$NO_2 + O_3 \rightarrow NO_3 + O_2$	DeMore, *et al.* (1994)
R15	$NO_3 + NO_2 + M \rightarrow N_2O_5 + M$	Atkinson, *et al.* (1992)
R16	$HO_2 + HO_2 \rightarrow H_2O_2 + O_2$	Atkinson, *et al.* (1992), Stockwell (1995)
R17	$H_2O_2 + h\nu \rightarrow 2OH$	DeMore, *et al.* (1994)
R18	$H_2O_2 + OH \rightarrow HO_2 + H_2O$	Atkinson, *et al.* (1992)
R19	$HO + HO_2 \rightarrow H_2O + O_2$	Atkinson, *et al.* (1992)
R20	$HO + HO \rightarrow H_2O + O$	Atkinson, *et al.* (1992)
R21	$HO + HO + M \rightarrow H_2O_2 + M$	Atkinson, *et al.* (1992)
R22	$CH_4 + OH \rightarrow CH_3 + H_2O$	Atkinson, *et al.* (1992)
R23	$CH_3 + O_2 + M \rightarrow CH_3O_2 + M$	Atkinson, *et al.* (1992)
R24	$CH_3O_2 + NO \rightarrow CH_3O + NO_2$	DeMore, *et al.* (1994)
R25	$CH_3O + O_2 \rightarrow CH_2O + HO_2$	Atkinson, *et al.* (1992)
R26	$CH_3O_2 + HO_2 \rightarrow CH_3O_2H + O_2$	DeMore, *et al.* (1994)
R27	$CH_3O_2H + h\nu \rightarrow CH_3O + OH$	DeMore, *et al.* (1994)
R28	$CH_3O_2H + OH \rightarrow CH_3O_2 + H_2O$	DeMore, *et al.* (1994)
R29	$CH_2O + h\nu \rightarrow CHO + H$	DeMore, *et al.* (1994)
R30	$CH_2O + OH \rightarrow CHO + H_2O$	Atkinson, *et al.* (1992)
R31	$CHO + O_2 \rightarrow CO + HO_2$	Atkinson, *et al.* (1992)
R32	$SO_2 + OH + M \rightarrow HOSO_2 + M$	Atkinson, *et al.* (1992)
R33	$HOSO_2 + O_2 \rightarrow HO_2 + SO_3$	DeMore, *et al.* (1994)
R34	$SO_3 + H_2O \rightarrow H_2SO_4$	Atkinson, *et al.* (1992)
R35	$CFCl_3 + O(^1D) \rightarrow$ products	DeMore, *et al.* (1994)
R36	$CFCl_3 + h\nu \rightarrow$ products	DeMore, *et al.* (1994)
R37	$CF_2Cl_2 + O(^1D) \rightarrow$ products	DeMore, *et al.* (1994)
R38	$CF_2Cl_2 + h\nu \rightarrow$ products	DeMore, *et al.* (1994)
R39	$N_2O + h\nu \rightarrow N_2 + O(^1D)$	DeMore, *et al.* (1994)
R40	$N_2O + O(^1D) \rightarrow 2NO$	DeMore, *et al.* (1994)
R41	$N_2O + O(^1D) \rightarrow N_2 + O_2$	DeMore, *et al.* (1994)

Table 2. Aqueous Phase Chemical Reactions Included in the Model

No.	Reactions
R42	$H_2SO_4(g) \Leftrightarrow H_2SO_4(aq)$
R43	$H_2SO_4(aq) \Leftrightarrow HSO_4^- + H^+$
R44	$HNO_3(g) \Leftrightarrow HNO_3(aq)$
R45	$HNO_3(aq) \Leftrightarrow NO_3^- + H^+$
R46	$CH_2O(g) \Leftrightarrow CH_2O(aq)$
R47	$SO_2(g) \Leftrightarrow SO_2(aq)$
R48	$SO_2(aq) \Leftrightarrow HSO_3^- + H^+$
R49	$HSO_3- \Leftrightarrow SO_3^= + H^+$
R50	$H_2O_2(g) \Leftrightarrow H_2O_2(aq)$
R51	$HO(g) \Leftrightarrow HO(aq)$
R52	$HO_2(g) \Leftrightarrow HO_2(aq)$
R53	$HO_2(aq) \Leftrightarrow H^+ + O_2^-$

All rate constants from Pandis and Seinfeld (1989).

Latitude

Figure 1. Latitudinal distributions of relative emissions (0-1) of $CFCl_3$, CF_2Cl_2, N_2O, CO_2, CO, CH_4, NO_X, and SO_2.

Year   **Year**

Figure 2. Annual emissions of $CFCl_3$, CF_2Cl_2, N_2O, CO_2, NO_X, CO, CH_4, and SO_2.
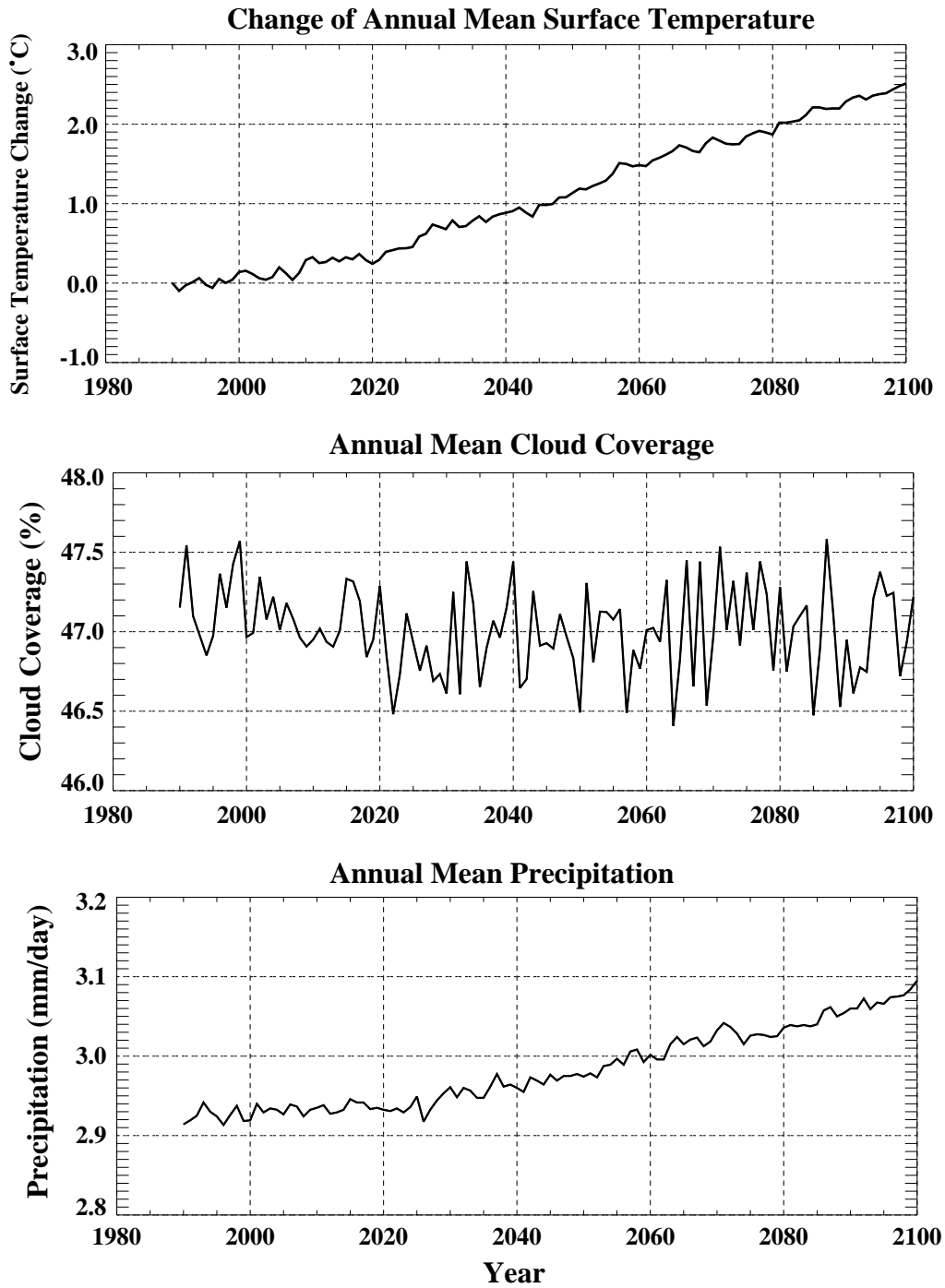
Figure 3. Model predicted annual-mean and global-average values of surface temperature (expressed as the changes from the 1990 level, top panel), cloud coverage (middle panel), and precipitation rate (lower panel).

19
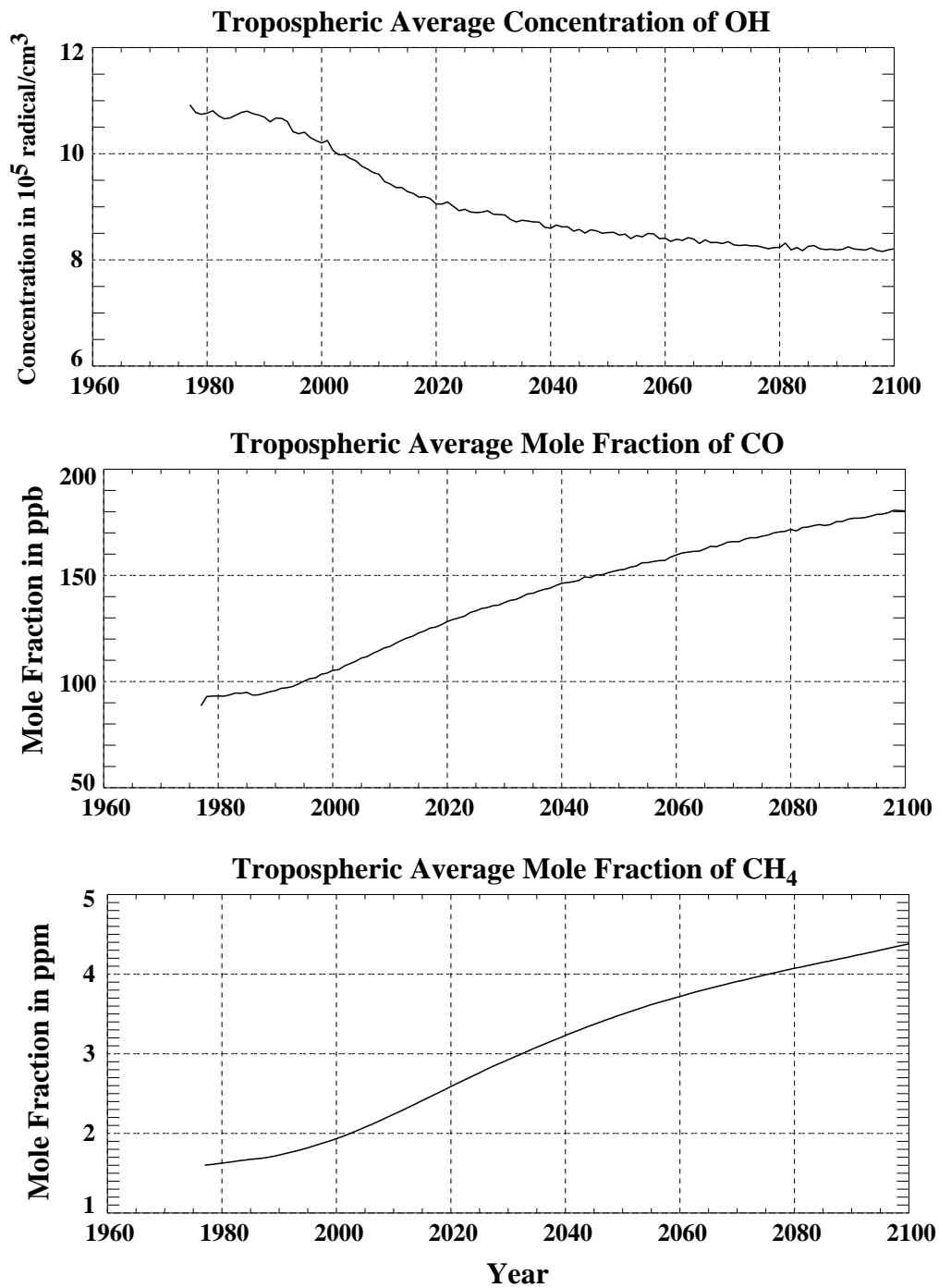
Figure 4. Model predicted tropospheric concentrations of OH (top panel), mole fractions of CO (middle panel), and mole fractions of CH$_4$ (lower panel), as functions of time.

CO Mole Fraction in ppb
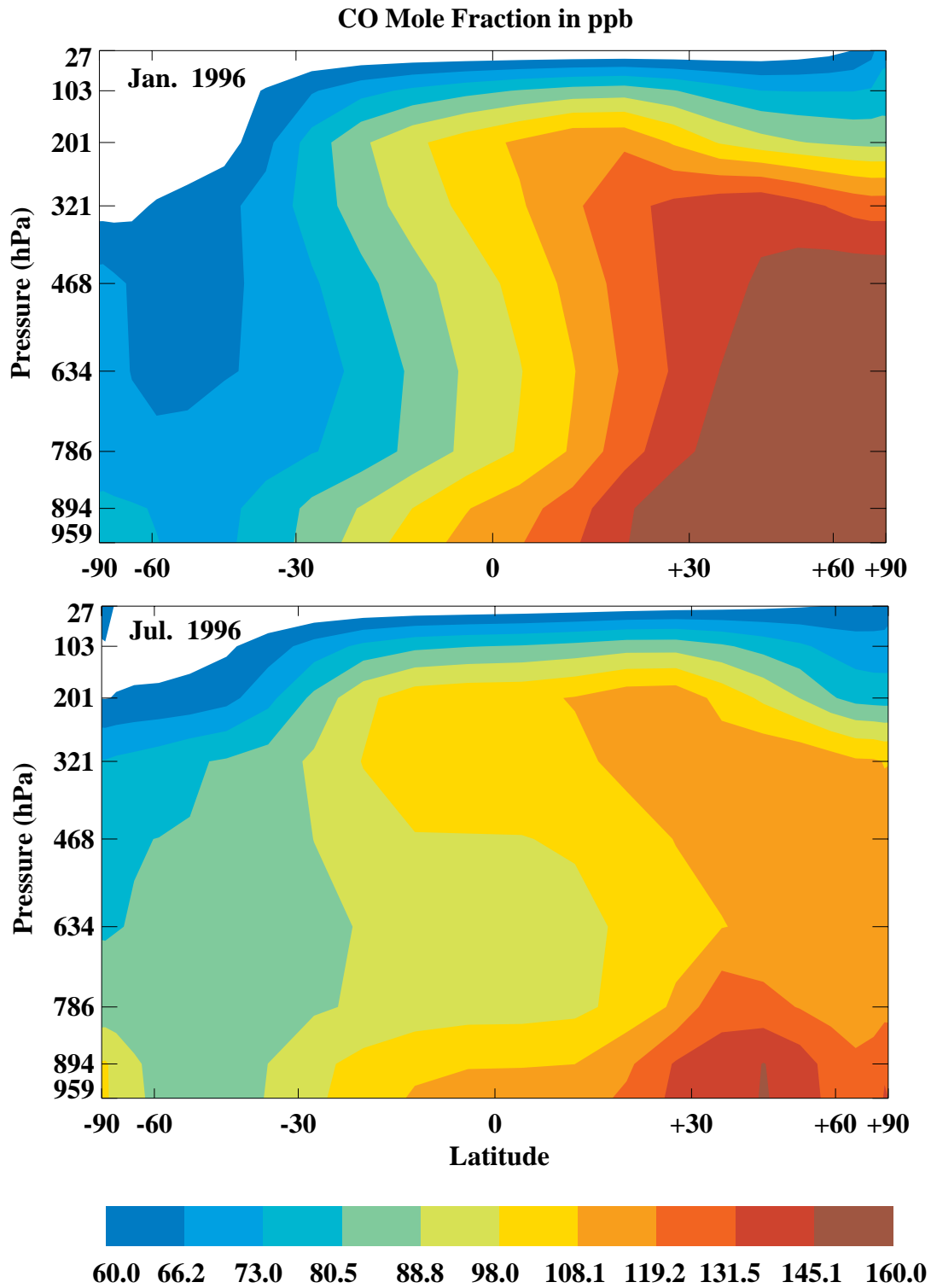
Figure 5. Model predicted latitudinal and vertical distributions of zonal average mole fractions of CO in January (top panel) and July (lower panel) of 1996.

21

NO$_x$ Mole Fraction in ppt
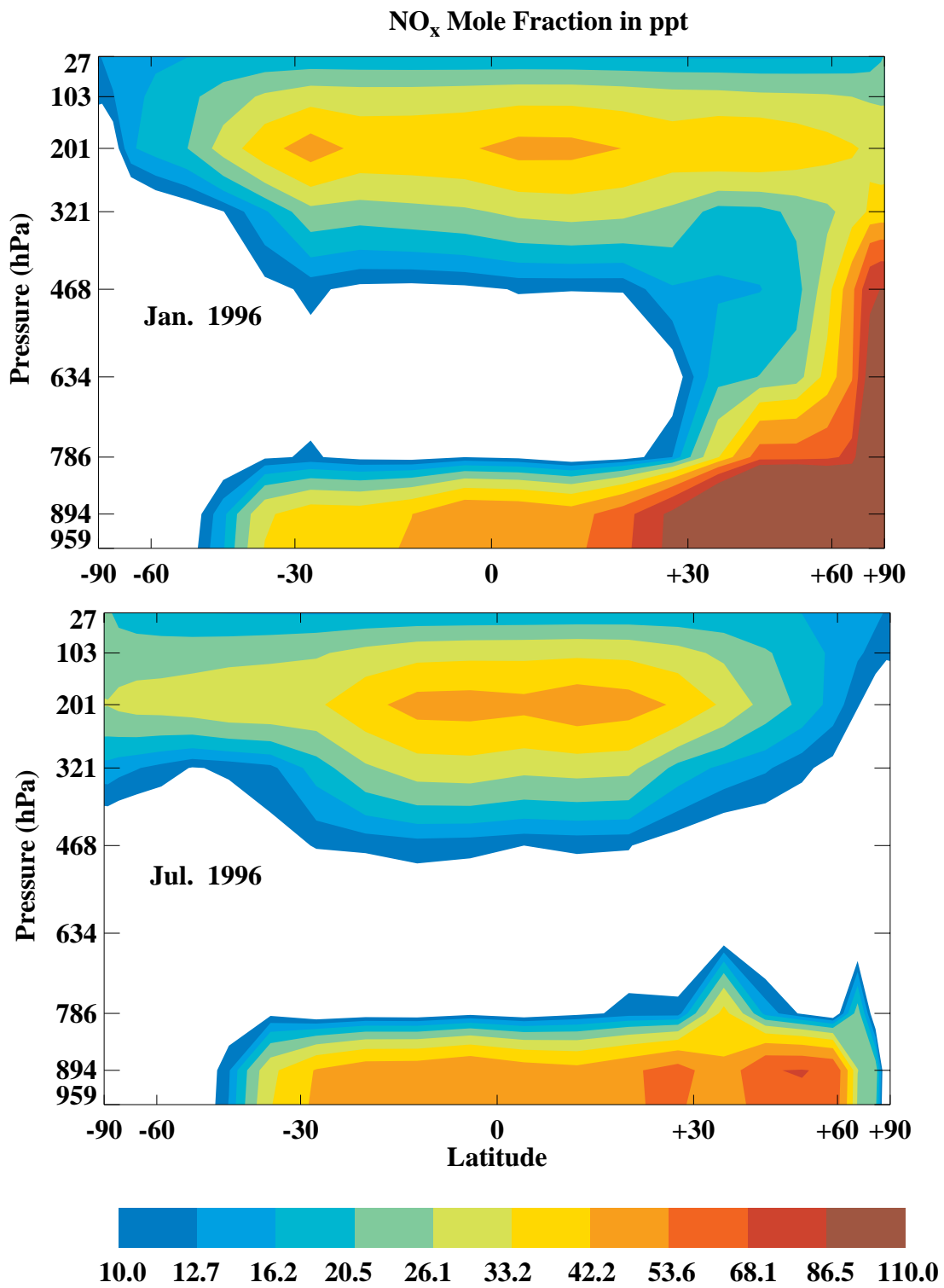
Figure 6. The same as in Figure 5, except for NO$_x$.
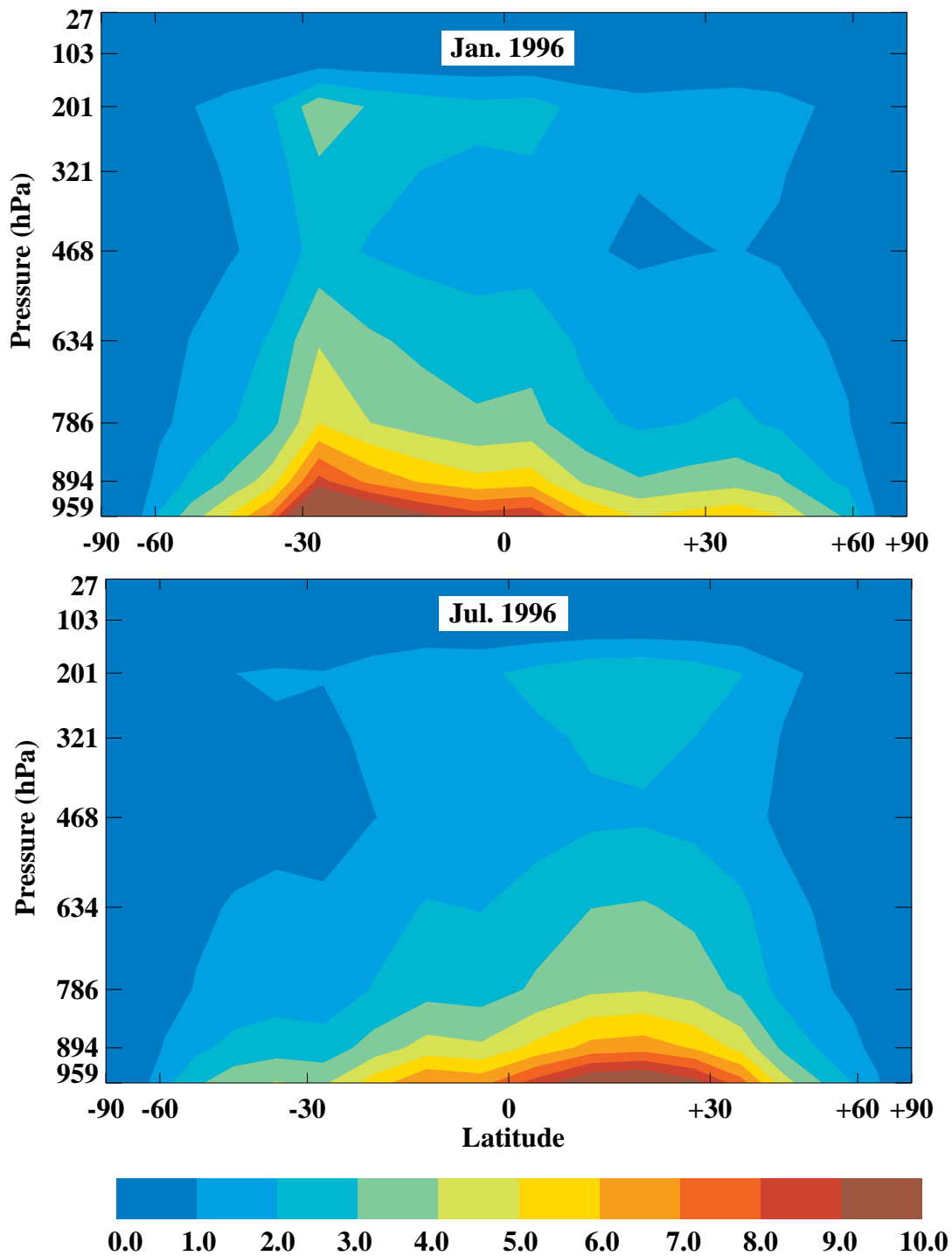
Figure 7. The same as in Figure 5, except for production rates of NO by lightning.

HO Mole Fraction in 10^{-3} ppt
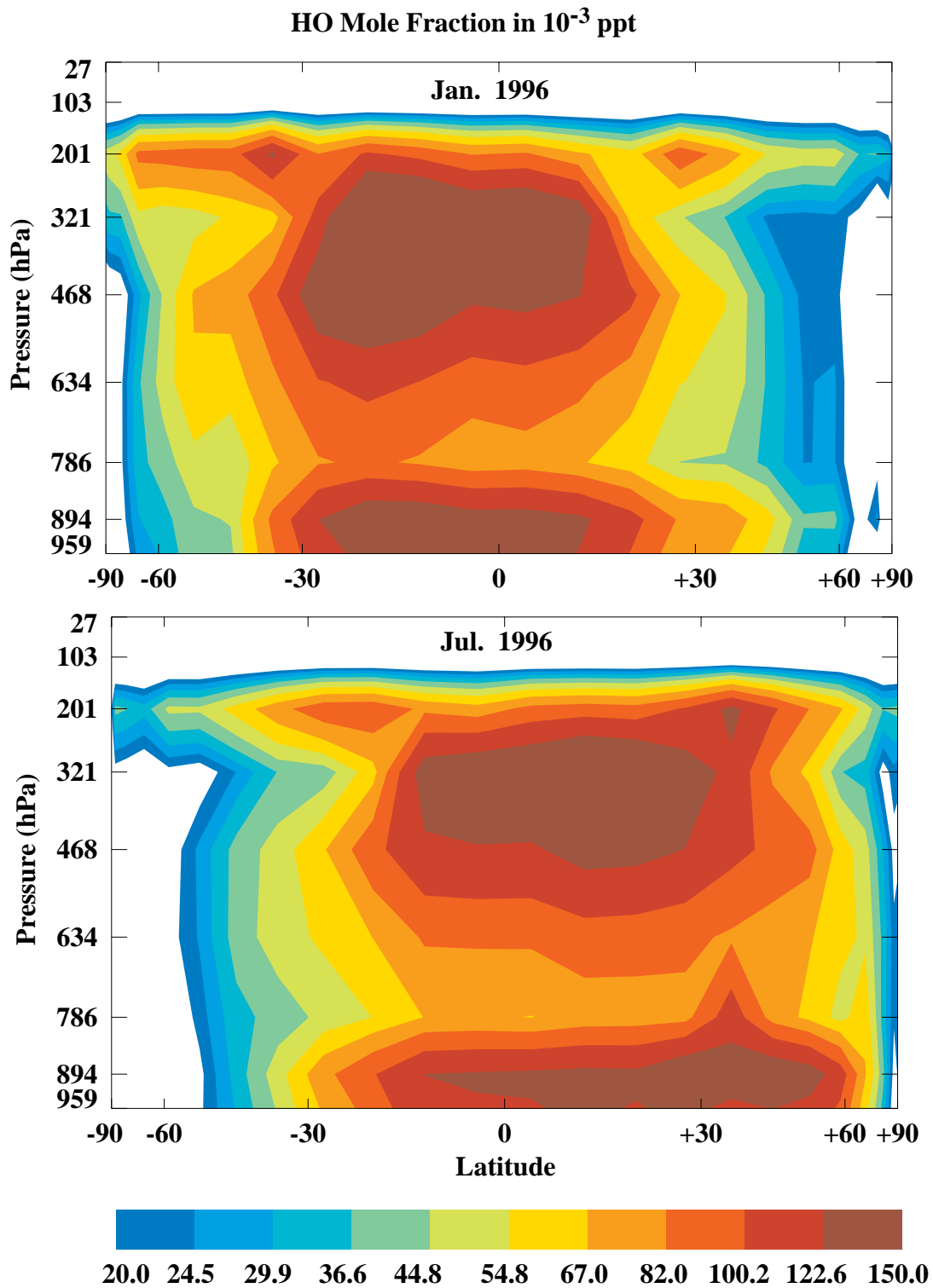
Figure 8. The same as in Figure 5, except for OH.

SO$_2$ Mole Fraction in ppt
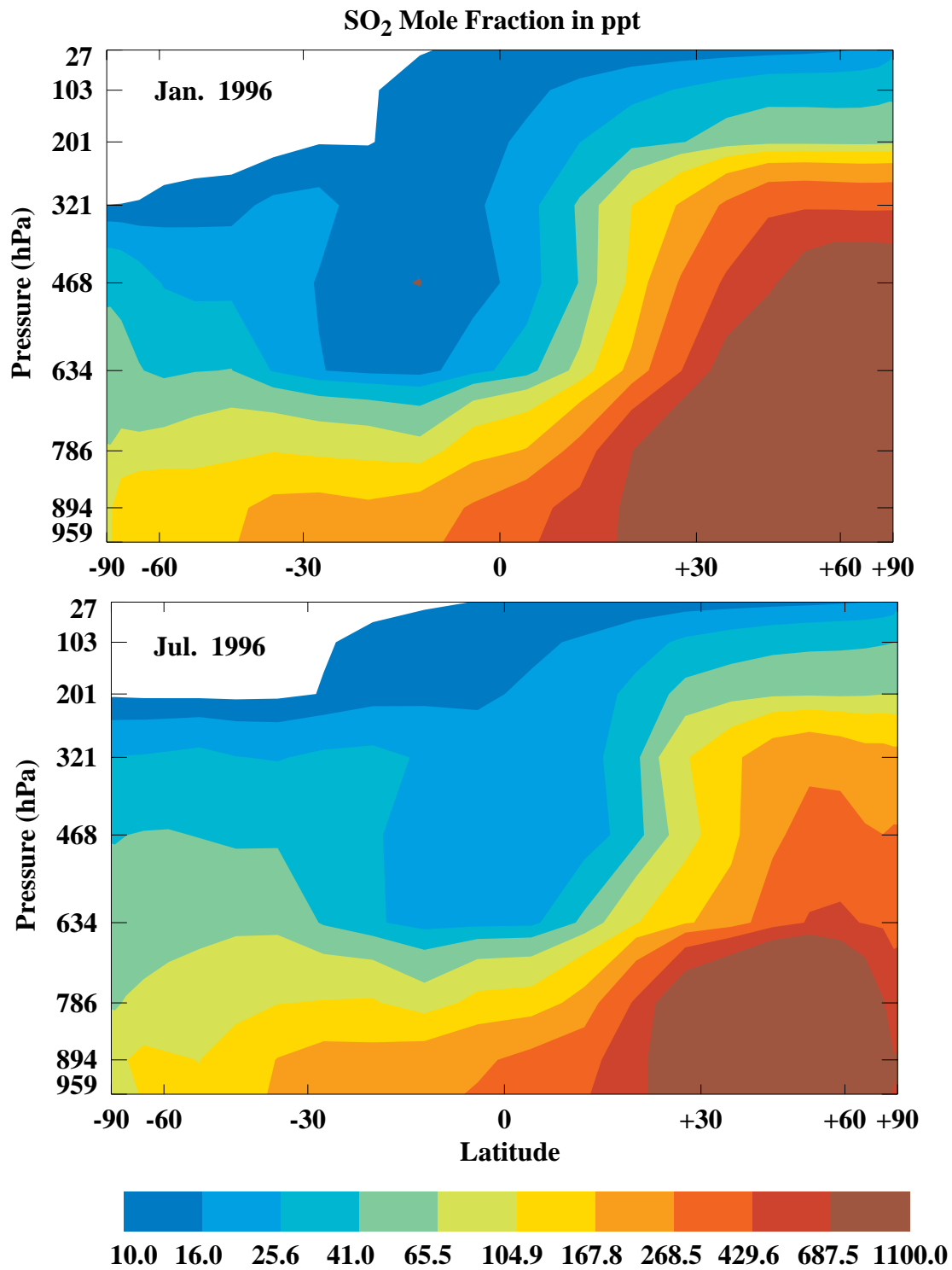
Figure 9. The same as in Figure 5, except for SO$_2$.
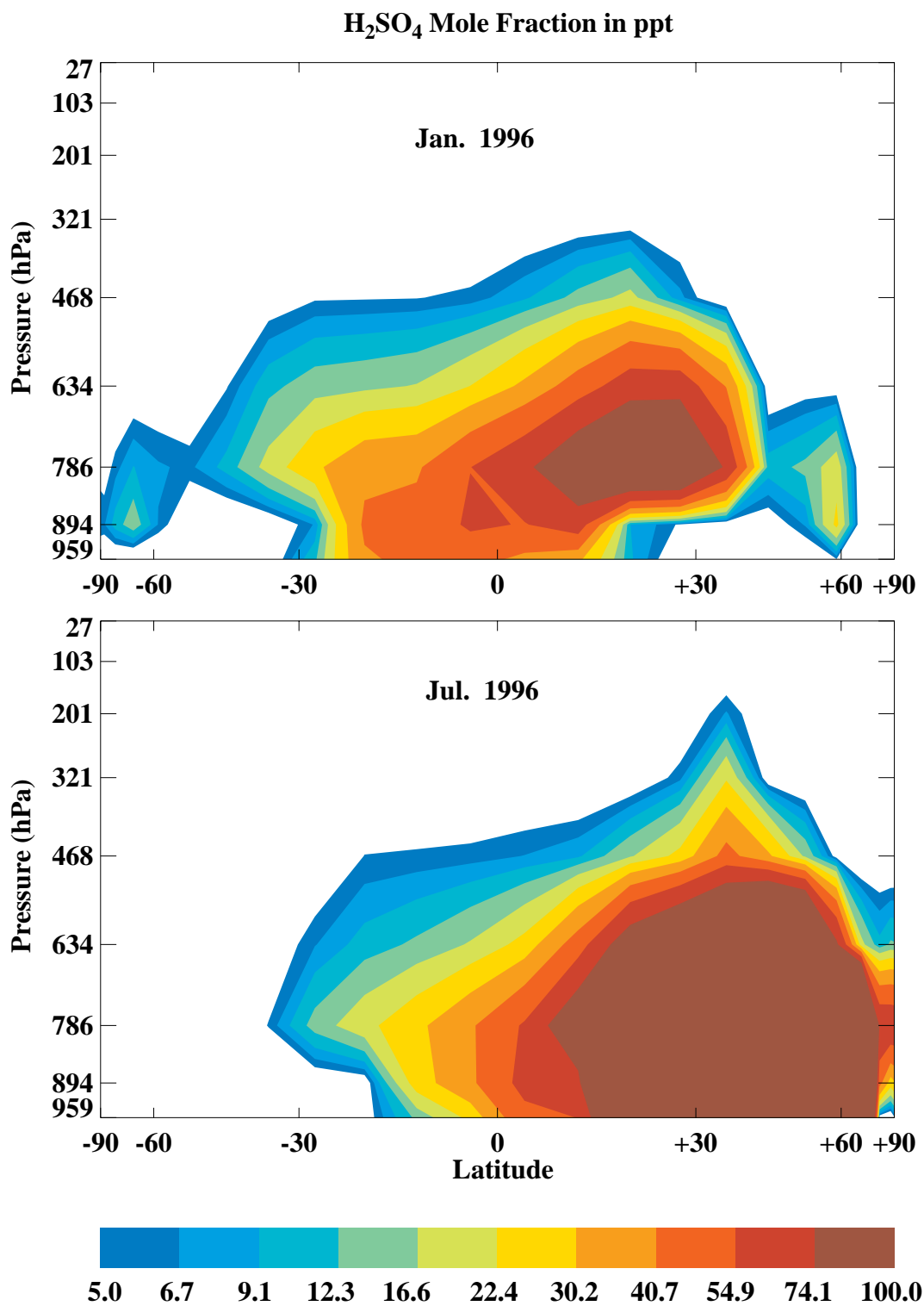
Figure 10. The same as in Figure 5, except for H_2SO_4.
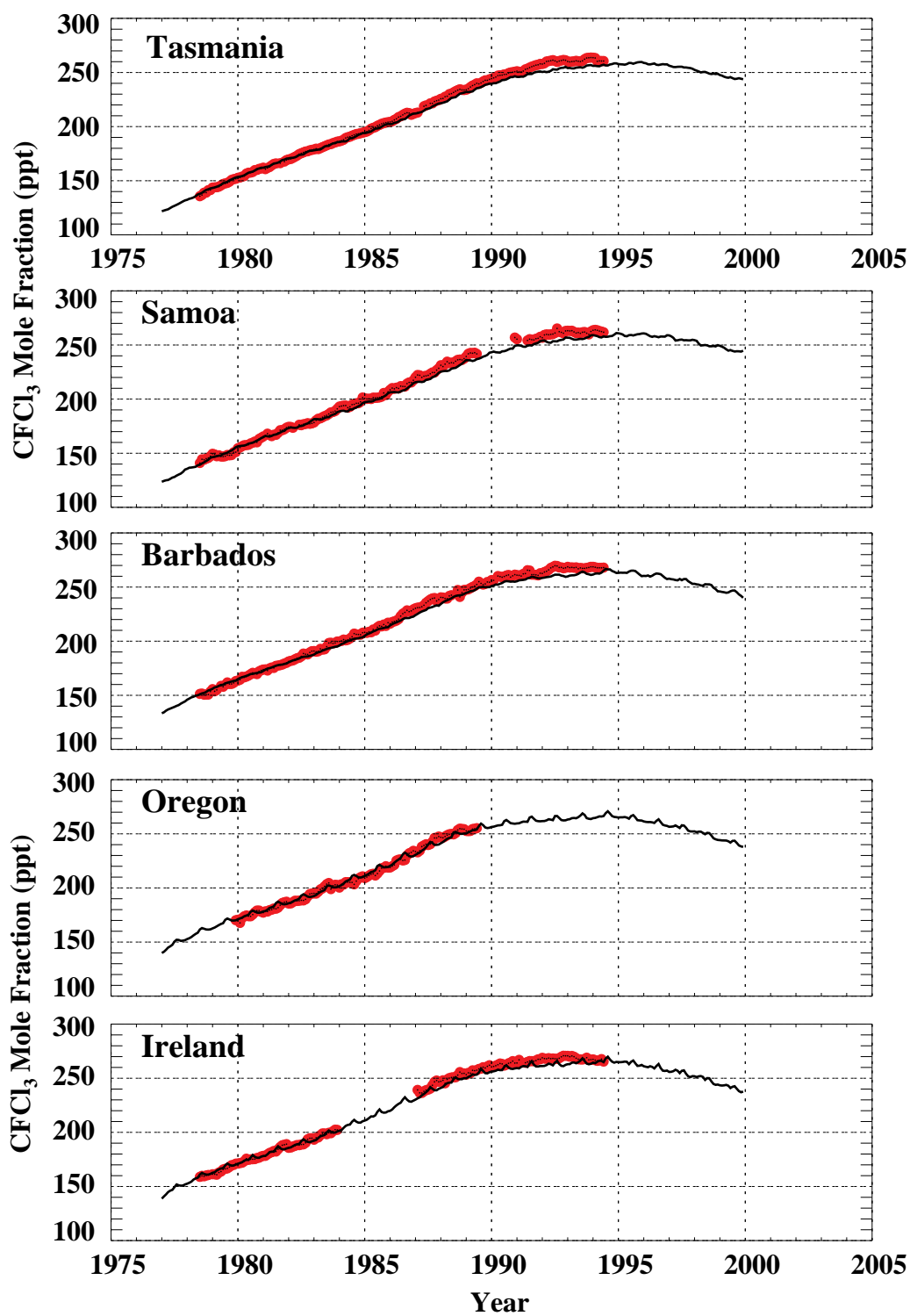
Figure 11. Comparisons between model simulated (lines) and observed (dots) surface mole fractions of CFCl$_3$ at five ALE/GAGE/AGAGE stations.
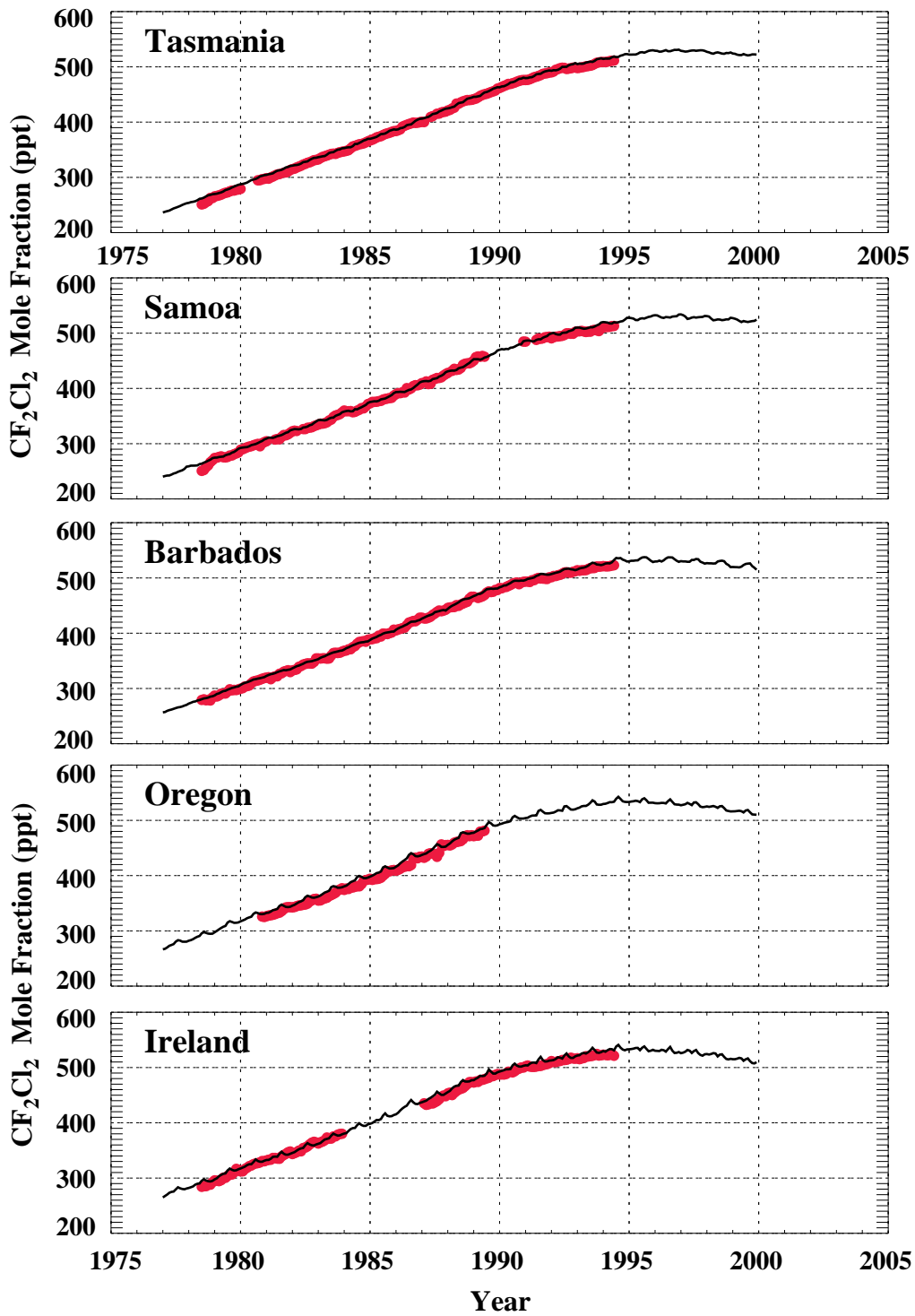
Figure 12. The same as in Figure 11, except for CF_2Cl_2.

28

CFCl₃ Vertical Distribution
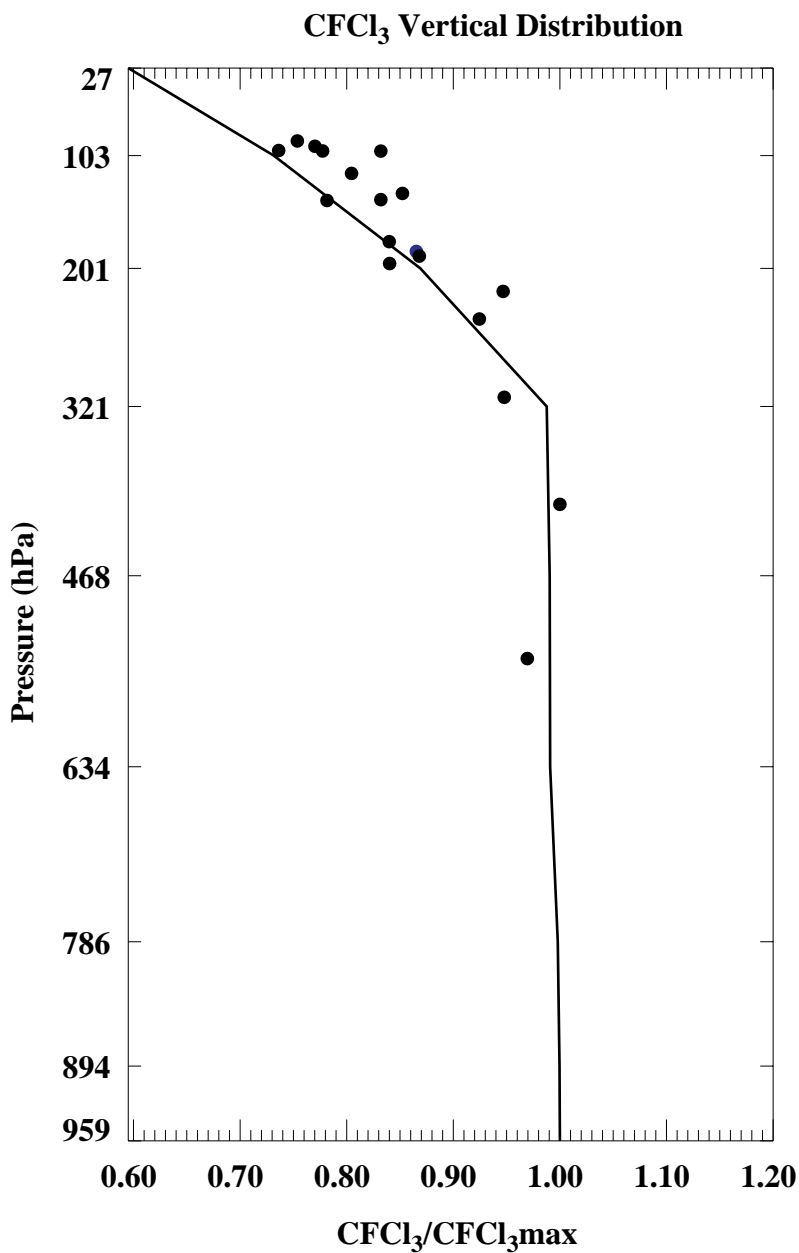
Figure 13. Comparison between model simulated (line) and observed (dots) vertical profiles of CFCl₃ at 44 °N. Observational data are from three balloon observations (June 20, 1989; November 5 and 10, 1990) by Ulrich Schmidt and co-workers as reported in Fraser, *et al*. (1994). The model data are averaged values from June 1989 to November 1990. Both observational and modeled concentrations are expressed relative to the maximum values in each profile (CFCl₃/CFCl₃max).
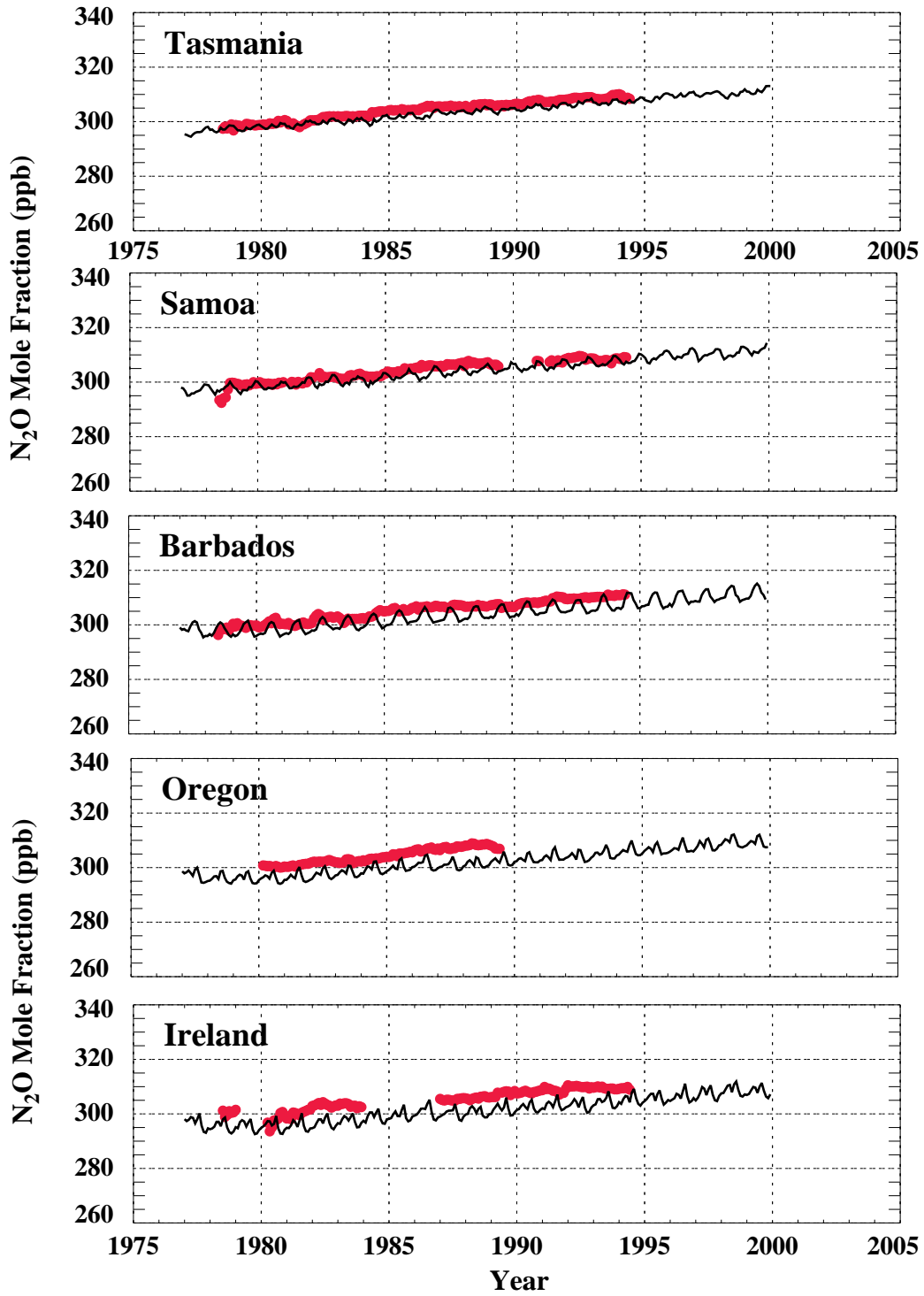
Figure 14. The same as in Figure 11, except for N$_2$O.
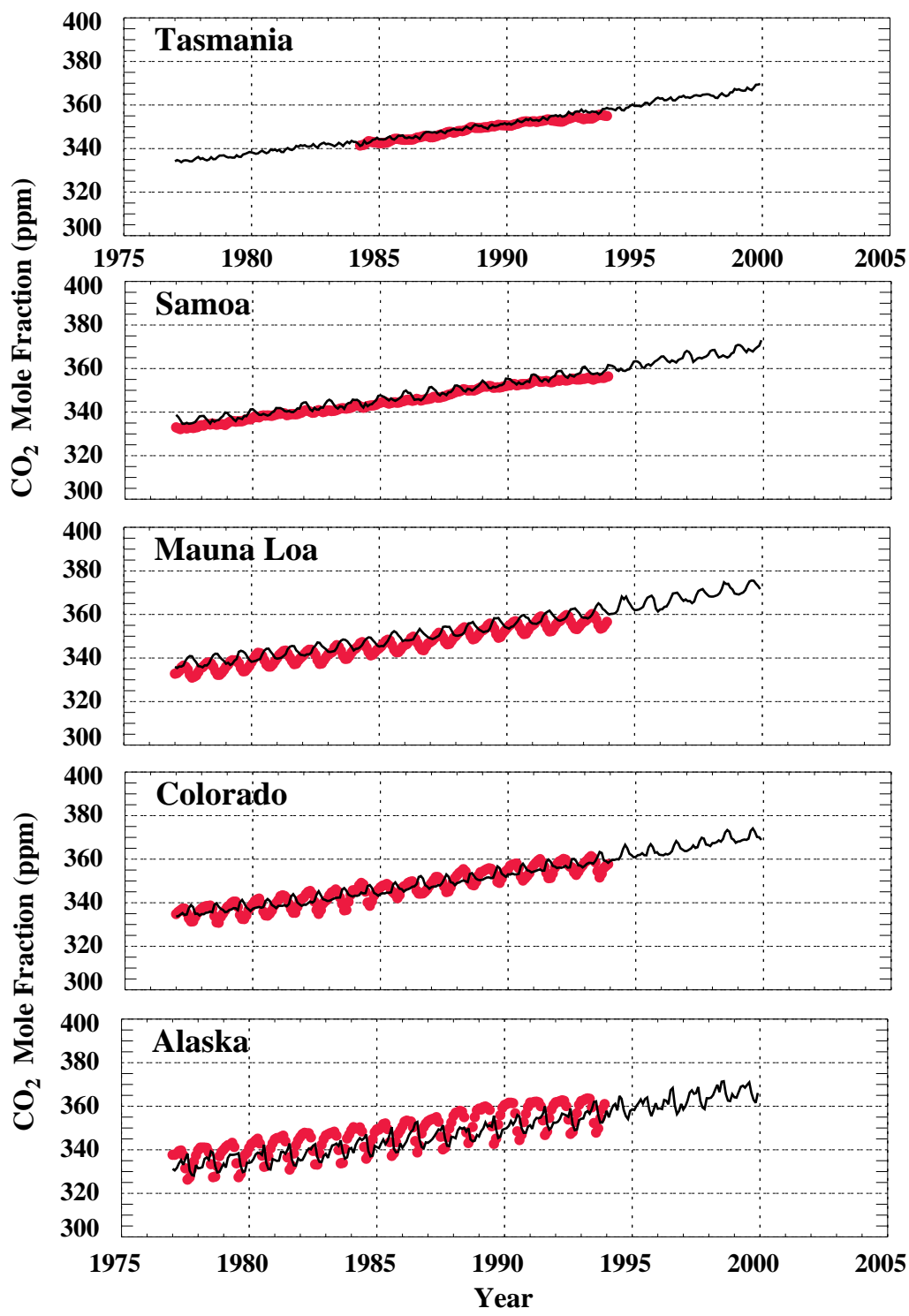
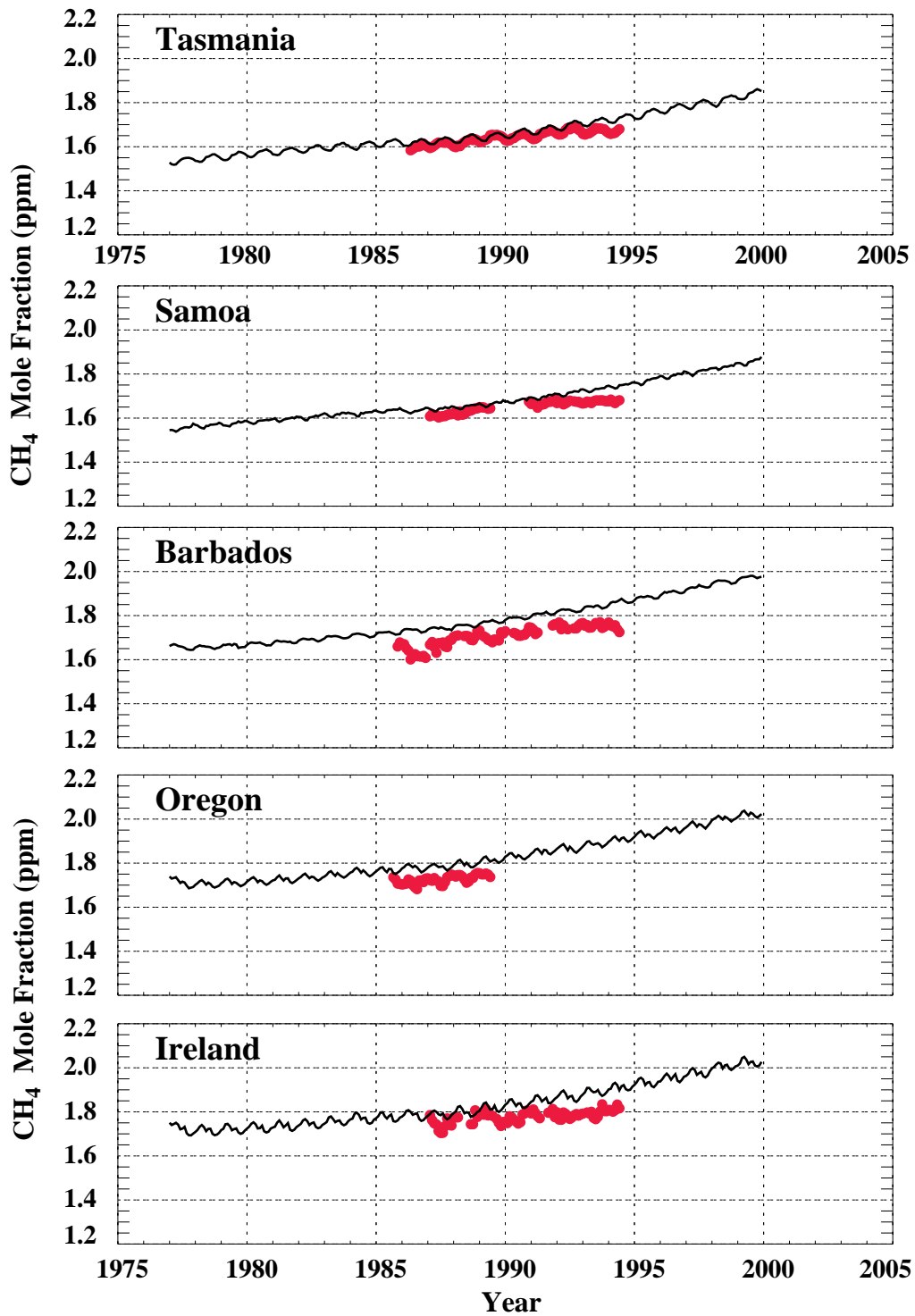**Figure 15**. The same as in Figure 11, except for CO_2 at five NOAA/CMDL stations.

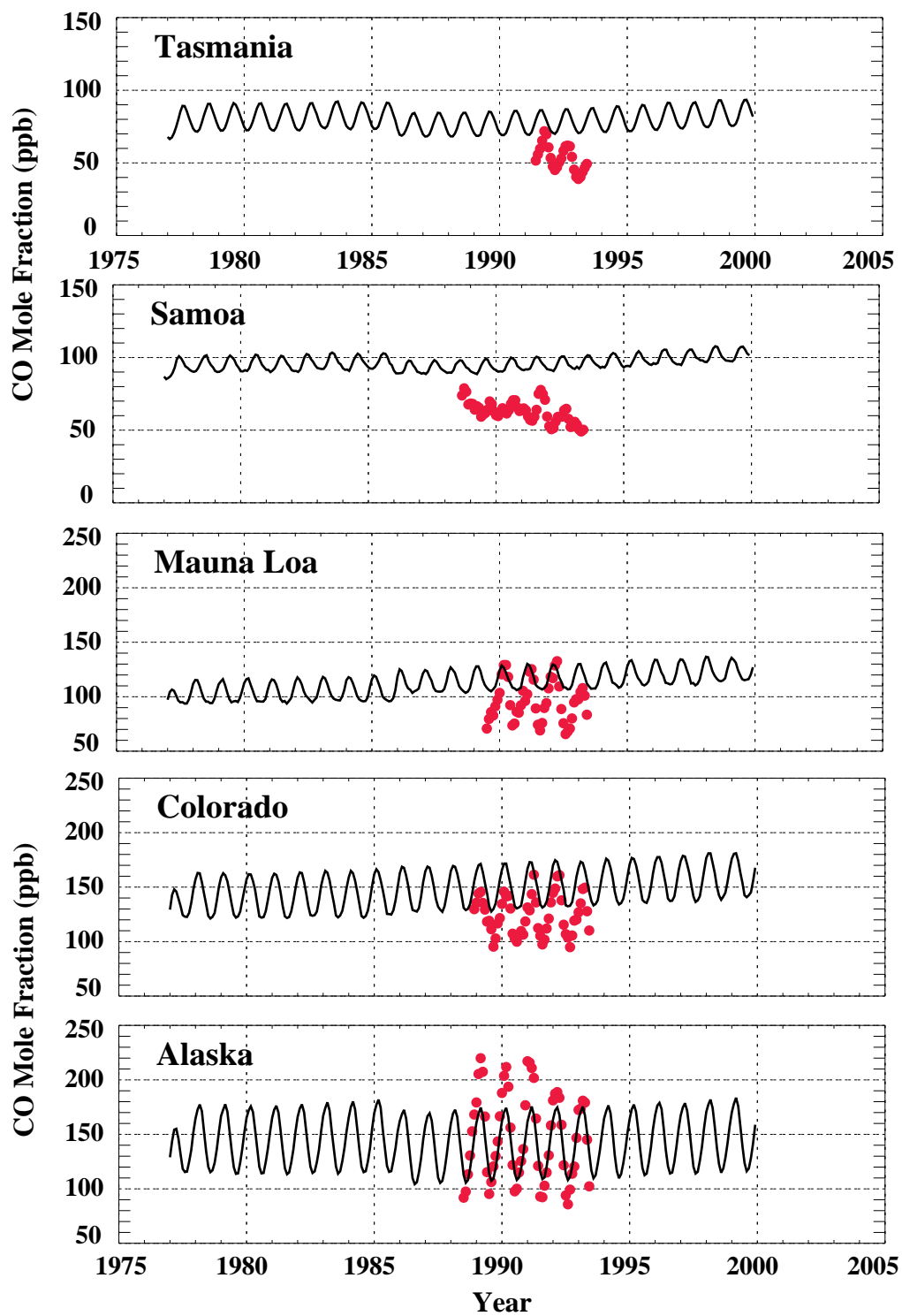**Figure 16**. The same as in Figure 11, except for CH$_4$.

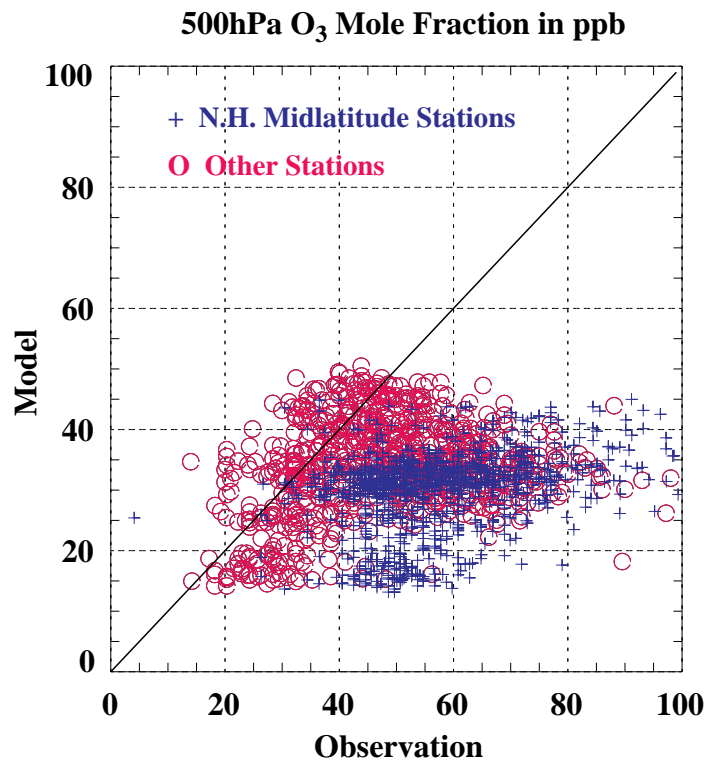**Figure 17**. The same as in Figure 11, except for CO at five NOAA/CMDL stations.
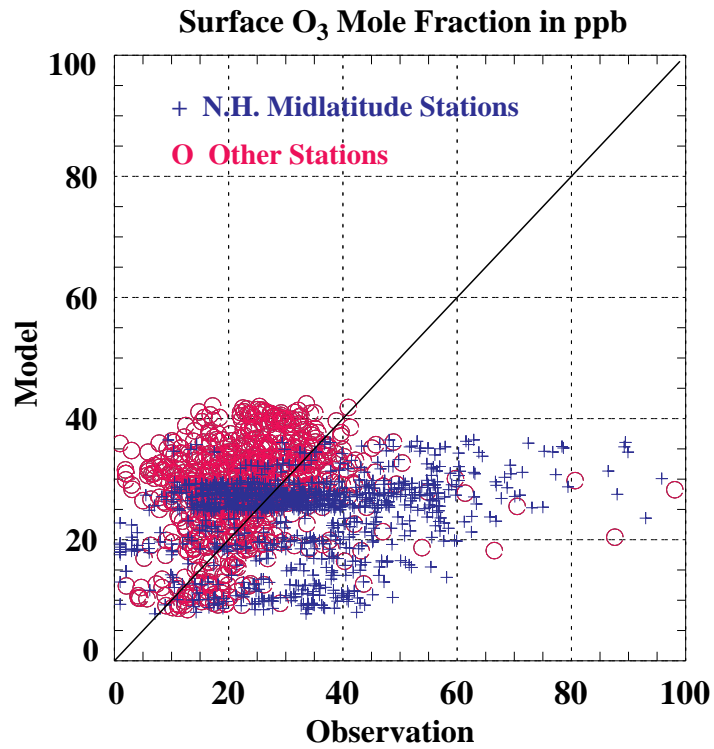
Figure 18. Comparisons between modeled and observed ozone mole fractions at surface (top panel) and 500 hPa (bottom panel) levels. Data from the Northern Hemisphere midlatitudes are marked by red circles, data from other stations are marked by blue crosses. Observational data are from 22 ozone sounding stations archived in the World Ozone Data Center (WODC).